THE HONG KONG
POLYTECHNIC UNIVERSITY
香港理工大學
Pao Yue-kong Library
包玉剛圖書館

Copyright Undertaking

This thesis is protected by copyright, with all rights reserved.

By reading and using the thesis, the reader understands and agrees to the following terms:

1. The reader will abide by the rules and legal ordinances governing copyright regarding the use of the thesis.

2. The reader will use the thesis for the purpose of research or private study only and not for distribution or further reproduction or any other purpose.

3. The reader agrees to indemnify and hold the University harmless from and against any loss, damage, cost, liability or expenses arising from copyright infringement or unauthorized usage.

Pao Yue-kong Library, The Hong Kong Polytechnic University, Hung Hom, Kowloon, Hong Kong

http://www.lib.polyu.edu.hk

MICROSPHERE ENHANCED OPTICAL NEURAL STIMULATION AND PHOTOACOUSTIC NEURAL RECORDING

FEI CAO

PhD

The Hong Kong Polytechnic University

2021

The Hong Kong Polytechnic University

Department of Biomedical Engineering

Microsphere enhanced optical neural stimulation and photoacoustic neural recording

Fei Cao

A thesis submitted in partial fulfillment of the requirements for the degree of Doctor of Philosophy

January 2021

ABSTRACT

Understanding the roles of neurons on behavior requires precise perturbation and fast reading of neural activity during ongoing behavior. Optical techniques stand out of other modalities regarding the cell-type/circuit specificity and the ability to both polarize and depolarize neurons with high spatiotemporal resolution. Optogenetics, relying on fiber optics and light-sensitive neural actuators, has revolutionized the neural stimulation field making it possible to precisely investigate a certain neural function in a casual manner. Optical reading, based on neural-activity-sensitive indicators integrated with fluorescent sensors and working with various optical configurations, brings molecular-level understanding of brain functions. Despite tremendous developments in superficial cortex, the inherent strong light attenuation in tissue remains a major challenge for interrogation of deep brain regions.

The opaque scalp and skull are first two parcloses that block light to penetrate the brain. The brain tissue itself, is lipid rich and highly turbid in which photons can hardly go very far (more than 200μm) ballistically. For optical stimulation, conventional optogenetics uses a fiber inserted into the cortex for delivering sufficient light power to a specific brain region. Effects of tissue scattering is added to the natural conical divergence of light from the fiber tip output, making the power density exponentially reduced to below the threshold which is needed to influence neural function in a sufficient brain region to induce behavior. In this case, strong power density is always

required ($>100\text{mW/mm}^2$) at the fiber tip for successfully driving a behavior, which results in several side effects, such as heat induced neural damage and "escaped" photons induced retina excitation and background noise behaving. For optical recording, non-ballistic photons act as major role in blurring an image and decrease the signal-to-noise ratio. The imaging depth and recording sensitivity is therefore greatly limited.

In this thesis, efforts are made to circumvent the scattering induced light attenuation in brain tissue in both stimulation and recording aspects. Firstly, a microsphere-enhanced optogenetic method is demonstrated exploiting the photonic nanojet effect. The converging profile, i.e., the photonic nanojet is simulated regarding various microsphere sizes and refractive indices to select a most appropriated sphere parameter for experiments. Then by using the transparent polystyrene microsphere, the enhancing ability is studied systematically, from *in vitro*, *ex vivo*, to *in vivo* demonstrations. Results show that microspheres facilitate driving comparable neural response and behavior with much less stimulation power. Secondly, a wearable photoacoustic imaging device for neural calcium imaging is designed and fabricated. The photoacoustic effect is introduced and exploited expecting less scattering from the acoustic side compared to pure optics. Both i*n vitro* and *in vivo* studies are conducted demonstrating feasibility of the idea. The great potential for combining these two studies in this thesis to form a closed-loop neural interrogation technique is finally discussed to open other possibilities in neuroscience research.

Key words: light attenuation, scattering, microsphere, optogenetics, photoacoustic imaging

ACHIEVEMENTS ARISING FROM THE THESIS

Journal Paper

1. **Cao, F**.; Qiu, Z.; Li, H.; Lai, P., Photoacoustic Imaging in Oxygen Detection. Appl. Sci. 2017, 7, 1262.

2. Zhou Yingying*, **Fei Cao***, Huanhao Li, Xiazi Huang, Dongshan Wei, Lidai Wang, Puxiang Lai, Photoacoustic imaging of microenvironment changes in facial cupping therapy. Biomedical Optics Express 2020. (*Equal contribution)

3. Huanhao Li, **Fei Cao**, Yingying Zhou, Zhipeng Yu, and Puxiang Lai, "Interferometry-free noncontact photoacoustic detection method based on speckle correlation change," Opt. Lett. 44, 5481-5484 (2019)

4. Xiazi Huang, Wenting Shang, Han Deng, Yingying Zhou, **Fei Cao**, Chihua Fang, Puxiang Lai, Jie Tian. Clothing spiny nanoprobes against the mononuclear phagocyte system clearance in vivo: Photoacoustic diagnosis and photothermal treatment of early stage liver cancer with erythrocyte membrane-camouflaged gold nanostars. Applied Materials today, 2019.

5. Lin Song, Guohao Wang, Xuandi Hou, Shashwati Kala, Zhihai Qiu, Kin Fung Wong, **Fei Cao**, Lei Sun, Biogenic nanobubbles for effective oxygen delivery and enhanced photodynamic therapy of cancer. Acta Biomaterialia, 2020.

Conference Proceedings

1. **F. Cao**, Z. Qiu, R. Zhang, P. Lai, and L. Sun, Nonlinear Photoacoustic Imaging by Pump-Probe Excitation. International Conference on Photonics and Imaging in Biology and Medicine, (Optical Society of America, 2017), paper W3A.79.

2. **Fei Cao**, Zhihai Qiu, Lin Song, Puxiang Lai, Lei Sun, Detection of oxygen level with photoacoustic imaging. International Conference on Biomedical Ultrasound 2017, P03.

3. **Fei Cao**, Zhihai Qiu, Kinfung Wong, Puxiang Lai, Lei Sun, "Nonlinear photoacoustic generation by pump-probe excitation," Proc. SPIE 10878, Photons Plus Ultrasound: Imaging and Sensing 2019, 108784R (27 February 2019).

4. Rui Zhang, Zhihai Qiu, **Fei Cao**, Jinghui Guo, Lei Sun, Study Piezo1 Localization and Transportation Dynamics by Light-sheet Microscopy. International Conference on Photonics and Imaging in Biology and Medicine, (Optical Society of America, 2017), paper W3A.89.

Academic award

1. Best Student Presentation Award by Chinese Society for Optical Engineering. International Conference on Photonics and Imaging in Biology and Medicine, 2017.

ACKNOWLEDGMENTS

First and foremost, I would like to express my sincere gratitude to my chief supervisor Dr Lei Sun. He guides me to distinguish all kinds of sceneries in the academic path and appreciate the beautiful ones. He teaches me not to believe authorities without critical thinking. He tells me that sky is the only limit and supports me to be explorative and try ambitious ideas as I can think of. He reminds me one should live up to his conscience. Everyone can be a teacher in life, but the one that spotlight your inner world is a mentor.

I am deeply thankful to my co-supervisor Dr Puxiang Lai. I have been working in his lab for most of my time. He is always supportive to my ideas and willing to try his best to help me. He took each of my manuscripts seriously and always gives valuable suggestions. He has also shared with me a lot of his experience in life and in academic path and encourages me a lot during the journey.

I would like to express my deep thankfulness to my family for their everlasting support. The invaluable things my parents give me are freedom and positive attitude towards life. They respect my thoughts and plans, and never try to control me with their expectations or programs. My brother has acted as important role during my growing up. He is seven years older than me has shared with me many of his experiences and views. These things together seeded optimism inside me and has been the inexhaustible power source that help me tide over any difficulties.

TABLE OF CONTENTS

LIST OF FIGURES

XIV

LIST OF TABLES

Introduction to the thesis background and structure

The brain has the most complex structure and function in the living body, which act as the headquarters and receive and analyze information, then give order and drive behavior. The brain is believed to be the "ultimate frontier" for understanding the nature and humanity itself. Integrated understanding from the molecular, cellular, systematic, and behavioral level is desired to reveal the true world of brain, which is far beyond the current cognitive level of human beings. The United States has pioneered the Human Brain Project (HBP) since early 1997 aiming to facilitate interrogation, protection, and development of human brain from molecular level to system level, by combining neuroscience and informatics. NIH has launched Brain Initiative in 2013 seeking to uncover the link between brain function, behavior and cognition, through supports from multi-disciplinary teams and collaborative efforts, finally improve treatment of brain disorders and development of artificial intelligence. Referring to mission of the Brian Initiative project, developing new technologies, tools and methods is of high priority as a small step that we can achieve in a short period rather than unpractical questions such as to draw a complete and precise picture of the activities of each neuron involved in brain activities.

In recent years, the development of technologies in neuroscience can roughly be divided into three categories, i.e., stimulation, recording, and analysis. Instead of conventional electrical stimulation which directly insert an electrode to a brain region, new

modalities include optogenetics by using genetically encoded opsins and sonogenetics by using genetically encoded mechano-sensitive proteins to drive neural activities, and magnetic stimulation taking advantage of the strong penetrability and slow attenuation of the magnetic fields. Behind all the efforts exists the deep pursuit of noninvasive and precise brain stimulation which can finally be translated to clinical treatment and other realistic applications. Neural recording has developed from single electrode to collect signal from only one neuron to tens to thousands of micro-electrodes together to record signals from multiple neurons, thus giving more accurate description of brain activity in this small recording region. Developments of genetically encoded calcium indicators (GECI) and genetically encoded voltage indicators (GEVI) has greatly boosted development of reading neural activity. These indicators normally are optical-based and combine a sensor with a fluorophore, which change the fluorescent intensity upon binding ion or changing of membrane potential. Studies have tried by using miniature implantable lens combined with multi-photon fluorescence for less invasive imaging of neural firing in a relatively deep region. To minimize invasiveness, MRI, PET, and ultrasound-based/ -related techniques for directly monitoring neural activity, although in an infant stage, show good prospect in the future. With development of big-data analytics, huge information from imaging platforms, electrophysiological platforms, as well as cellular biological platforms could be integrated and analyzed to understand the realm of the brain fast and unambiguously, and at the same time facilitating diagnosis

of neural disorders by artificial intelligence.

Among modalities mentioned above, optical based techniques for both neural stimulation and recording represent a unique direction. Three major advantages of light make it a powerful tool for neuroscience. First of all, visible and IR light is non-ionizing and non-carcinogenic, which is safe for human. Secondly, light occupies a very small but important region in the electromagnetic spectrum that can interact with molecules of interest exclusively and gives biochemical molecular specificity which is unable to realize by other modalities. In addition, the spatiotemporal resolution with millisecond time control and single-neuron localization of light-based methods is much superior to others. Harnessing these characteristics and fiber optics, optogenetics has revolutionized neuroscience toolbox by making it possible to excite or inhibit specific neurons with no interference of other neurons, which was never achieved by other methods before its development in 2005. On the other side, optical imaging and recording systems keeps iterating aiming at uncovering brain activity at high-resolution and in large-field-of-view. These techniques have greatly promoted new discoveries in superficial brain regions. Huge amount of information from deeper brain regions, however, remains to be interrogated and is facing major challenges. In optogenetic stimulation, the descending power density with depth beyond the fiber tip quickly drops to below the stimulation threshold, thus hinders light-neuron interaction in depth. On the other side, the intrinsically strong light scattering in biological tissue distorts the

beam path and further reduce the power density, which weaken the ability of both fiber-based stimulation and recording. These problems exist as big obstacles in the way of progress from study of rodents' brain to primate brain which has much larger size and higher-level functions such as concept of number and calculation, self-awareness, etc., those are close to functions of human brain.

This thesis targets the light attenuation problem and develops microsphere-assisted optogenetic stimulation and photoacoustic neural recording. Starting with a review about the development of neural modulation and recording modalities and optics-based stimulation and recording of neural activity in Chapter 1, the fundamental challenges in front of this thesis work is clearly recognized and light scattering theory and its role in biomedical applications are introduced to elaborate on the problem we are facing. Chapter 2 details the exploitation of microsphere and the photonic nanojet effect in optogenetics, both simulation and experimental results are included. Chapter 3 gives design and preliminary demonstration of noninvasive photoacoustic neural recording for behaving study. A conclusion and an outlook are finally followed up in Chapter 4.

Chapter 1 Development of neural modulation and recording modalities

1. Characteristics of neuron and the dissecting concept

The nervous system plays a centra role in leading the physiological functional regulation and controlling activities in the body. Large numbers of neurons gather to form all kinds of circuits in the central nervous system (CNS) and function as carriers to store, process and transmit information, generating a variety of psychological activities, and control all the behavior of animals. Neurons transmit information electrically within the neuron in the form of action potential and chemically to the adjacent neuron by chemical messengers. Recording of action potential in 1939[1] by inserting micro-electrodes into the giant axons of squids has started the era of electrophysiology. The development of patch clamp in late 1970s and early 1980s, which also won the 1991 Nobel Prize in Physiology or Medicine, has for the first time enabled currents recording from single ion channel during the action potential process. These works have laid the foundation and paved way for interrogation of single neuron property and the snowballing development of neuroscience and neuroengineering.

Under the resting state, healthy neurons have membrane potential at approximately -85mV to -60mV from inside of the cells by assigning the extracellular fluid as voltage zero, and generally hold steady[2]. Upon disturbance by local electrical currents that is

above the threshold (-55mV), the neuron is activated to an excited state and start firing, as shown in Figure 1, by redistribution of three major mobile ions, Na^+, Cl^-, and K^+. In this state, the membrane potential normally reaches +30mV to +40mV, and then quickly back to its resting state in millisecond and get ready for another firing. This action potential can propagate along the axon without attenuation till to the synapse, where voltage-gated Ca^{2+} channels open and trigger neurotransmitter to release to excite or inhibit the downstream neuron. This whole process is repeated on the downstream neuron once its dendrite receives the neurotransmitter and get "disturbed". In a large scale, groups of neural response orchestrally may create oscillations and rhythms which induce local field potential (LFP)[3], brain-wide activity, and finally behavior.
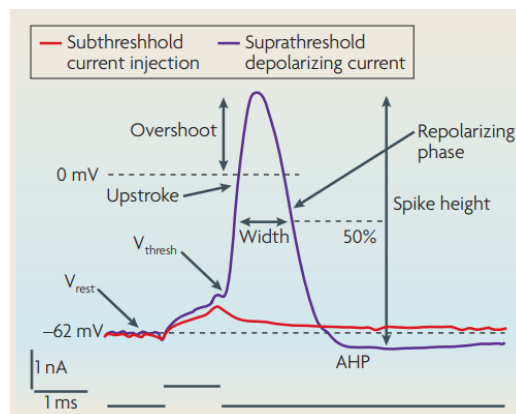
Figure 1 A representative action potential profile when disturbed by a local electrical current[4].

Action potential is the fundamental of neuroscience and from which developed both neural stimulation and recording techniques for causal unraveling of neural function as well as diagnosis and treatment of neural disorders. Figure 2 shows a typical closed-loop neural instrument including body-electrode interface for transporting stimulation

and sensing neural electrical activity; controller for switching between stimulator mode and recording mode; data transferring, processing, and storing components; and power supply. There's a trend in taking the idea of a closed loop including stimulation and feedback, and then adjusted stimulation with using a cluster of newly developed perturbation and recording techniques rather than by using electrodes alone to provide more detailed information in depth in order to better understand the brain and to restore brain functions or prevent pathological conditions, such as MRI guided brain stimulation[5] and all-optical electrophysiology[6, 7]. The combination of stimulation with imaging methods to monitor neuronal activity, will have a major impact in neuroscience.
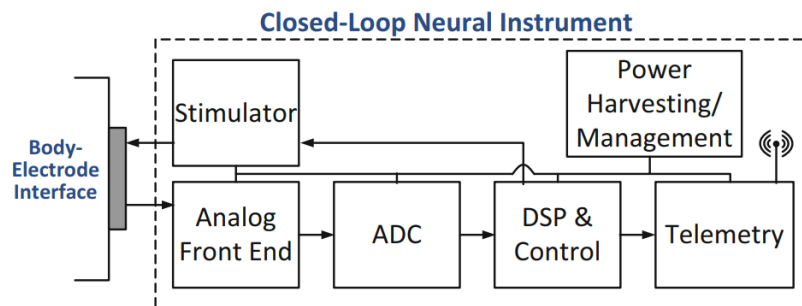
Figure 2 A typical closed-loop neural instrument including body-electrode interface for transporting stimulation and sensing neural electrical activity [8]

2. Development of neural stimulation

The most widely used is electrical stimulation and recording which has profound influence in prostheses and treatment. The first recorded electrical stimulation dates back to 46 AD on a torpedo fish[9]. The technique has then been more and more applied

in various fields. In deep brain stimulation (DBS), an implantable pulse generator is used to continuously deliver electrical pulses. DBS is a promising treatment for movement disorders of Parkinson's disease, dystonia, and essential tremor, which has been approved by the US Food and Drug Administration (FDA). DBS was reported to have larger than 50% of improvement in patients with movement disorders[10]. However, conventional DBS implementation includes chronically implanted electrodes which may induce chronic safety issues, the invasiveness is facing more and more challenges with developing noninvasive brain stimulation modalities. Transcranial magnetic stimulation (TMS), transcranial electrical stimulation (TES) and focused ultrasound stimulation (FUS) are representatives of non-invasive and less painful stimulation. TMS employs pulsed magnetic fields to induce eddy currents in the brain and subsequential physiological responses are expected to affect brain metabolisms and neural activities, in which low frequency stimulation patterns induced cortical inhibition and the high-frequency stimulus pattern causes excitation. TES delivers an electrical current through the cortex for restoring brain function especially of those suffering from mental illness such as brain damage or severe depression. Ultrasound can propagate and penetrate through biological tissues through the skull, and the energy can be focused into a small volume in sub-millimeter scale, thus as an alternative to eliminate the risks of implanted hardware.

The neural specificity, however, are as low the same in these techniques. The

macroscale electrodes used in DBS are very likely to non-selectively stimulated adjacent neurons, thus playing as a limiting factor for improving DBS treatment efficiency, inducing additional motor control effects and sensory problems. TMS, TES and FUS meets the same problem in clinics. Resonant magnetic imaging (MRI) is normally used as a guidance for targeting an appointed brain region due to the matched spatial resolution between MRI and FUS. Towards cellular-scale neural specificity and selectively excitatory, inhibitory or combined control of neuronal activity, FUS and optogenetics (OG), chemogenetics (CG)/ pharmacogenetics (PG)[11] methods have been developing fast in recent years, harnessing mechano-sensitive and optical-sensitive ion channels, respectively. Figure 3 shows a comparison of the specificity between electrical and optogenetic stimulation. These channels are genetically encoded to the cell membrane, and only can be opened upon stimulation from the right energy at appropriate parameters (e.g., Light/ ultrasound (in FUS) frequencies and power density/ pressure). Pharmacogenetic approaches can activate opsins chemically and hence eliminate fiber implantation and multi/ constant stimulation which is superior to optogenetics alone in this respect. However, its benefit is still controversial, and the spatial and temporal precision are not easy to control. Development of light induced photothermal[12] and photoelectrochemical[13] by using materials with broadband absorptions or ultrasound induced mechano-thermal neuromodulation provide nongenetic neural control. Besides, as heating can be effective for a distance up to

100um, the thermo-based mechanism is ideal for peripheral nerve stimulations[13].

Combination of physical and biotechnological neuromodulation techniques will greatly

facilitate clinical translation of these techniques[5].

Table 1 summarized current brain stimulation modalities used in clinics as well as in

developing.
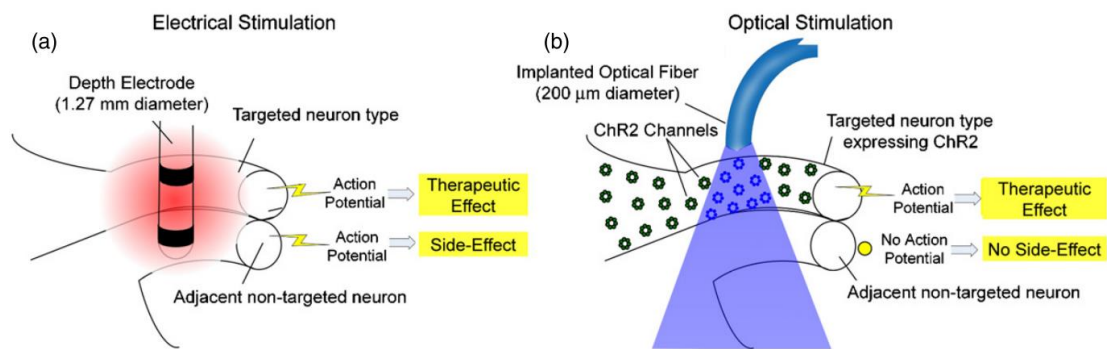
Figure 3 Comparing the cell specificity between electrical and optogenetic stimulation (a) Electrical stimulation affects all types of cells near the electrode non-specifically. (b) Optogenetic stimulation only interacts with neurons of a specific type that have been genetically targeted by expressing opsins (ChR2 in this figure). Schematic not to scale.[14]

Table 1 Current brain stimulation modalities

	Spatial precision	Temporal precision	Invasiveness	Cell-type specificity	Neural depolarization	Neural hyperpolarization
DBS	mm	ms	Yes	Low	Yes	No
TMS	cm	ms	No	Low	Yes	No
TES	mm	ms	No	Low	Yes	No
FUS	μm~mm	ms	No	High	Yes	Yes
CG/PG	mm~cm	min	No	High	Yes	Yes
OG	Single cell	ms	Yes	High	Yes	Yes

3. Development of neural recording

Understanding the brain function is of great importance in neuroscience. The advanced neural recording or imaging methods are crucial to the study of central nervous system in cognitive, systematic, or molecular and cellular level. Real-time functional information from neural recording is vital evidence to understand the mechanisms and real-time response behind neural activities in terms of behaviors and thoughts. Over the past decades a wide variety of techniques for recording of neural activities have been developed, which differ in spatial scale, temporal resolution, and purpose. They can be categorized into electrophysiological methods, ionizing radiation methods, magnetic resonance methods, ultrasonic methods, and optical methods.

For the most widely used electrical methods for brain signal recording, the trade-off between anatomical coverage and spatiotemporal resolution is obvious. Electroencephalography (EEG) generally is used to measure the electrical fields in extracellular space with a coarse spatial and excellent temporal resolution (~10ms) and can only register large brain areas (whole brain) with collective neural dynamics[15]. Micro-electrocorticography (μECoG) can distinguish faster (~1ms) and smaller brain (1 mm^2- 10 cm^2) signals with increasing recording channels and thus smaller recording region[16]. Towards finer resolution (0.1ms) to cellular scale (100 neurons), multi-electrode arrays (MEA) with penetrating shanks for cortical neurons *in vivo* or benchtop MEA systems for brain slices or neural cultures have greatly contribute[17]. The

ultimate method and golden standard has been single-cell, even single-channel patch clamp recording (0.1ms)[18], as mentioned above.

Besides the above trade-offs, EEG is mostly used through scalp and noninvasively, but only pick up faint and low-frequency signals due to distances between electrodes and neurons. This not only make the signal hard to be localized, but also vulnerable to ocular artifacts[19]. To be close to neurons and get more specific high-frequency signals, the electrodes must be implanted into the brain, which is invasive and may cause other safety effects. In this case, the compromise between spectral range and invasiveness in these electrode-based recording techniques due to the natural low-pass filtering property of biological tissue [20] is another issue.

Other recording techniques in major include several imaging modalities, i.e., X-ray computed tomography (X-ray CT), functional magnetic resonance imaging (fMRI), positron emission tomography (PET), single photon emission computed tomography (SPECT), diffuse optical tomography (DOT), or magnetoencephalography (MEG) to image the brain structures and functions directly or indirectly. X-ray CT, PET and SPECT represent early development of neural imaging instruments in the 1980s and continue to contribute tremendously to neuroscience and diagnosis. Nevertheless, X-ray is an ionizing source in the electromagnetic spectrum and patients are normally exposed to significantly high dose of radiation which is 100-500 times higher than normal X-rays[21]. PET/ SPECT usually provide functional information with injection

of radioactive tracers. Although having good contrast and sensitivity when proper tracer is used, spatial and temporal resolution is always the main drawback. Moreover, the use of radioactive isotopes may cause radiation ionizing. Due to less invasiveness, low radiation exposure, non-ionizing contrast and wide availability, fMRI obtains blood oxygen level–dependent (BOLD) signal during neural activity relying on paramagnetic properties of oxygenated hemoglobin (HbO) and deoxygenated hemoglobin (Hb). By using magnetic fields and radio waves instead of X-rays or radioactive tracers, fMRI has dominated the brain imaging area since it is born in the 1990s with good spatial resolution and contrast, however, it provides low temporal resolution and moving of subject is prohibited. Comparably, DOT by using near infrared light and imaging the optical absorption of hemoglobin can generate similar results to fMRI[22]. The weakness of DOT is that it can only penetrate a few centimeters deep. MEG directly measures the magnetic fields induced by electrical stimulation and with less signal distortion than EEG. Ultrasonic method, with functional ultrasound (fUS) as a typical example, measures neural activities indirectly via blood volume. Though it has potentials of good spatiotemporal resolution and imaging depth, its actual utility is still under investigation. Photoacoustic imaging (PAI), as implicated by its name, combining optics and ultrasound has unique contrast with advanced spatiotemporal resolution. Table 2 summarizes the key properties of these brain imaging modalities.

Table 2 Key properties of brain imaging modalities. NA: not applicable.

	Spatial resolution	Temporal resolution	Penetrati-on depth	Contrast source	Directness to neural activity	Sensiti-vity	Safety	Weara-bility
EEG/MEG	10mm	ms	cm	Action potential	Yes	Depends	Safe	Good
X-ray CT	30-100μm	0.1s	cm-m	Anatomy	NA	NA	Ionizing	Poor
fMRI	mm	s-min	cm-m	Hemoglo-bin	No	Low	Safe with MR-safe body implants[23]	Poor
PET	1-2mm	0.3s	cm-m	Glucose metabolism	Yes	High	Radioactive	Poor
SPECT	1cm	0.3s	cm-m	Blood flow	Yes	High	Radioactive	Poor
DOT	One-third of imaging depth	ms	1-10mm	Hemoglo-bin	No	High	Safe	Good
fUS	50-200μm[24]	<1s[25]	cm	Blood volume	No	High	Safe	Good
PAI	0.1-200μm	50us	mm-cm	Molecule	Depends	High	Safe	Good

Having their own advantages and disadvantages as shown in Table 2 and in conventional optical methods mentioned above, these methods cannot meet full needs in the field of neuroscience. Despite bulky systems that are not wearable, new designs that the animals do not need to be anesthetized and can instead move freely during the experiments are more suitable for small animal in vivo behavioral and cognitive studies. Non-invasive and wearable system that allows free moving, deep brain penetration, high spatiotemporal resolution, and have access to neural functionality is on urgent developing.

4. Light-based neural stimulation and recording

Since development of the first laser in 1960, light has become a versatile tool and dramatically driven developments in multiple areas, such as physics, astronomy, telecommunication, accurate navigation, material manufacturing, and life science. The first trial by Fork in 1971 surprised the world by driving Aplysia abdominal ganglion neurons to the action potential threshold by focused laser[26]. With continuous optical technology development, direct two-photon stimulation of neurons with higher resolution and single-neuron potential *in vivo* was demonstrated in 2002[27]. Multi-disciplinary cooperation among physics, engineering, chemistry, and biology keeps impulsing development in neuroscience. Most early studies pay efforts to photo-stimulation with caged compounds such as glutamate[28] for mapping neural circuits. Although can be widely used since almost every neuron in mammalian CNS can be stimulated by glutamate, neuron type specificity and timing cannot be precisely controlled in this way as all cells can be excited near the stimulation site. On the other side, it is quite problematic to deliver these caged compounds *in vivo*. Towards high spatiotemporal precision, high neuron-type/network specificity, and flexible *in vivo* applications, selective neuron stimulation in a genetic-encoded way came into being.

Chosen as the Method of the year in 2010 by Nature Methods[29], "optogenetics has opened new doors for experimentation across biological fields". Optogenetics involves adaptation of microbial opsin genes encoded to neurons and light activation of optical

sensitive gene-encoded ion channels, as illustrated in Figure 4. From its emergence, optogenetics not only has been widely explored in neuroscience, but also shown great potential in treatment of neural disorders. The field keeps growing with efforts and developments in five major aspects, including opsins and channel-protein iteration, gene delivery system, light delivery system, neural activity reading, and applications in various body parts and disorders.
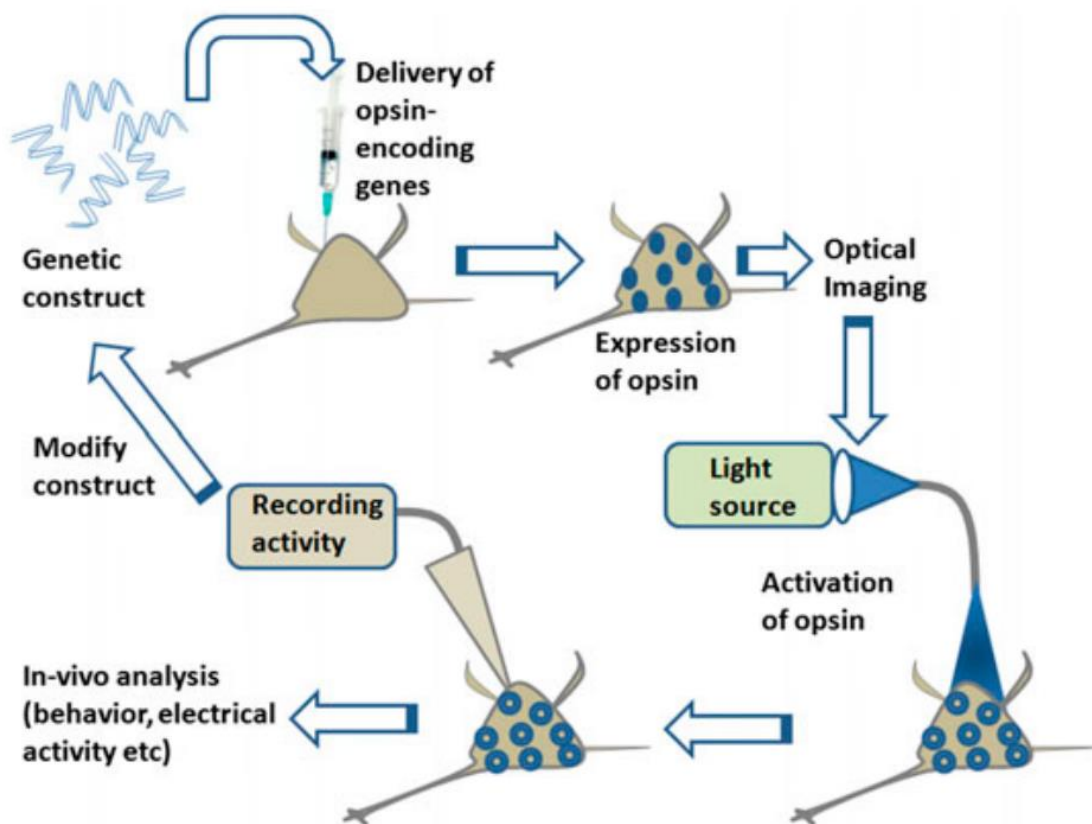
Figure 4 Illustration of optogenetic realization[30]. Gene modification combined with cell-type-specific promoters allow excitation (depolarization) or inhibition (hyperpolarization) of preselected neuron populations. Followed by confirming of successful expression of opsins on the cell membrane by fluorescence imaging, optogenetics is conducted to activate the opsins to elicit neural response or drive behavior. The stimulation results can be recorded for feedback instruction of next-round experiments.

Early genetically encoded optical studies[31-34], due their mechanisms for affecting depolarization, only allowed control of neuronal activity in timescales of seconds to minutes. Channelrhodopsin-2 (ChR2), through which cations stream into the cell membrane by responding to blue light, open the era of millisecond (a thousand time faster) control of single spikes and synaptic activity[35]. This improvement has brought optical stimulation to the speed that matches the fundamental building blocks of neural computation. In addition to neuron excitation, halorhodopsin (NpHR) inhibits neuron activity acting as a chloride pump upon shedding a yellow light[36]. Opsins are kept being reformatted through elaborate gene mutations (Figure 5). For example, to be more sensitive to light, thus enable deep penetration and large scale optogenetics[37, 38]; step-function opsins (SFO) to function longer time after stimulation to avoid consecutive high-power laser illumination and heating generation[39]; and to realize as fast as hundreds of hertz that can reach or even beyond the gamma band for more applications[40, 41]; or to response to red-shifted light wavelengths that are less absorbed or scattered and enables deep transcranial optical excitation[42]. The wavelength-dependent light interactions with opsins are shown with various colors in Figure 5.
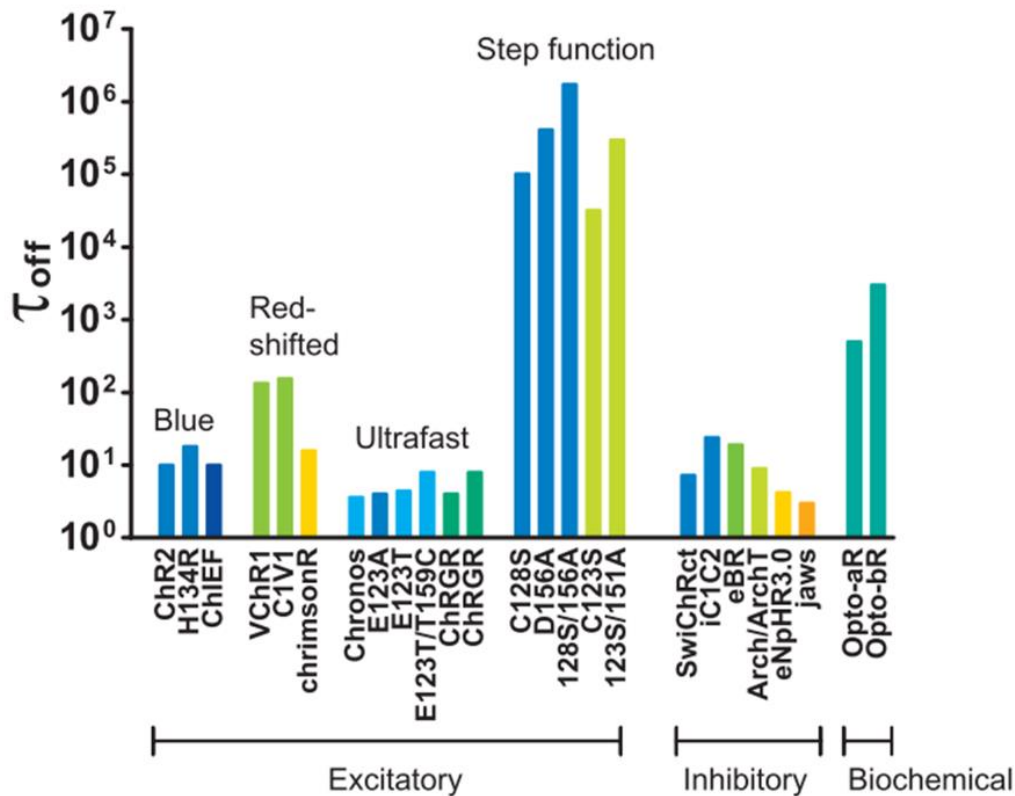
Figure 5 Some of the currently available opsins[43] with showing their corresponding functions (excitatory, inhibitory, or biochemical), off-kinetics, and responding wavelength.

Gene delivery system is developing from invasive ways to non-/less invasive ways. The light-sensitive proteins are generally introduced to targeted neurons via viral gene delivery approaches[35]. Due to existence of the blood brain barrier (BBB) and its natural blocking property, the most feasible route for viral delivery is direct brain injection and infusion[44]. Transgenic mice model[45] is an alternative approach that avoid brain injection and its related side effects, such as brain damage and vectors backflow, but operates at high cost due to the need for whole-body genome alteration. New techniques, for example by using MRI-guided transcranial focused ultrasound[46, 47] or shockwave[48] to open BBB, are kept emerging to be noninvasive, more cost-

14

effective and flexible. A newly developed virus that can cross the BBB and delivery genes throughout the CNS through intravenous injection[49] promotes noninvasive gene delivery technique a big step forward.

Light delivery system is an entirely distinct bioengineering challenge in optogenetics. The optogenetic efficiency is highly influenced by the protein expression extent on the target neurons as well as the number of photons that reach the opsin-expressing cells. Figure 6 illustrates two basic categories of light delivery. One is wide-field illumination which interact with all opsin-expressed neurons inside the propagation region (Figure 6 a)), this scheme is mostly used in in vivo studies by using an inserted optical fiber for free-behaving studies trying to correlate behavior to the brain function in a certain brain region. Given that neural cells within the same brain region may have diverse responding profiles [50-52], the other uses patterned light and interact with cells selectively as shown in Figure 6 b)). This strategy can be achieved with one-photon excitation (1PE) or two-photon excitation (2PE) combined with red-shifted channelrhodpsions for longer penetration depth and better 3D resolution. The neural events can be generated one by one by serially scanning of light beams or in parallel with structure modulated light beams. The neural events can be generated by one-opsin-one-wavelength combination, or multi-opsin-multi-wavelengths combination.
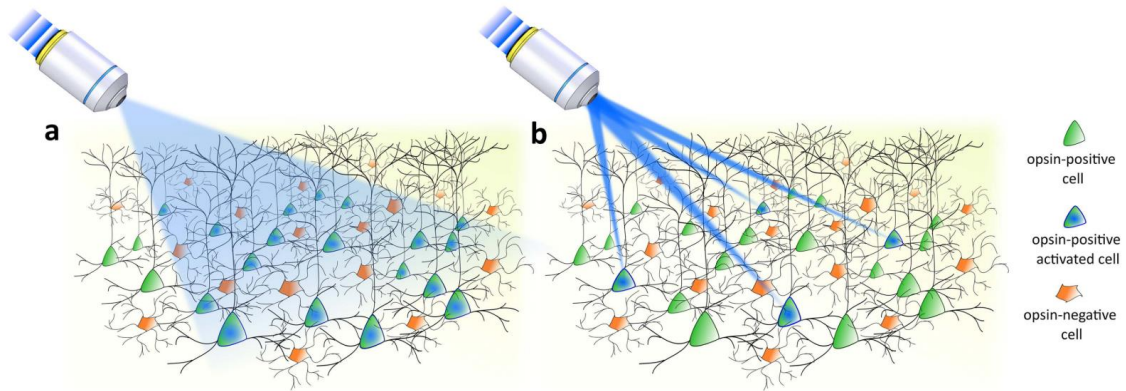
Figure 6 Illustration of two light delivery categories in optogenetics. (a) Wide field illumination and cell-type targeted optogenetics. (b) Gene- and light- double targeted single-cell resolution optogenetics[53]. Neural events can be generated with one-photon or two-photon interactions.

For the most common cases by relying on fiber optics for delivering light into brain. Although microfabricated waveguides (Figure 7a)) can delivery multiple individual light sources into the brain with a 2D[54]/ 3D[55] pattern to simultaneously or sequentially dissecting multiple cortical sites with cell-type specificity, and have the ability to address complex shaped and distributed neural circuits especially potentially helpful in large animals like primates, the complex optical patch for light coupling and scanning remain major drawbacks[56]. Implanting an optical fiber (Figure 7b) is still the most common light delivery method for both cortical and deep brain regions since demonstration in anesthetized[14] and freely behaving rodents[57]. Normally a step-index multimode fiber ceramic ferrule with 200μm core size is inserted into the brain cortex by using a stereotaxic instrument and through a hole on the skull. Dental cement is then used fixed the ferrule to the skull. A matching sleeve is used to connect the ferrule and patch cable only at experiment (Figure 7b)). Light-emitting diodes (LED)

or laser sources are then coupled into the fiber and animal can move freely with using a rotary joint. Towards wireless control and the most flexible movement, micro-LEDs integrated onto implanted devices also have been exploited[58, 59].
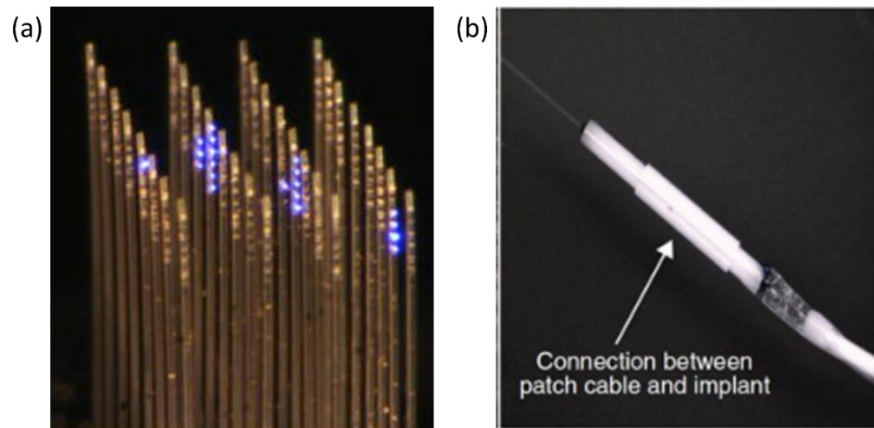
Figure 7 a) Optical micrography of 3D waveguide array with an DMD-modulated illumination pattern[55]. b) Implantable optical fiber ceramic ferrule connected with a patch cable [60].

The illumination pattern could be short light pulses with small duty cycles for excitation control, while continuous light for inhibition[61]. Sufficient power density (mW/mm^2) above a threshold is essential for successful stimulation, which depends on the specific opsin and its expression level. For wild-type ChR2, 1-5mW/mm^2 was found sufficient for ChR2-evoked action potentials[35].

Recording of neural activity is another essential technique concern in light-neuron interaction. Current optical techniques for neural recording can be generally categorized into two types. One features noninvasive, deep-penetration, and imaging of intrinsic contrasts *in vivo*. This type is represented by laser doppler flowmetry (LDF)

for measuring cerebral blood flow[62], near-infrared (NIR) spectroscopy for measuring oxygenated hemoglobin and deoxygenated hemoglobin changes during functional brain activation[63], function optical coherence tomography (fOCT) for detecting scattering changes during neural activation[64], and surface plasmon resonance (SPR) which is sensitive to refractive index changes during neural activities[65]. These optical cortical functional mapping has been used since the 1980s and developed dramatically afterwards. Being able to monitor brain physiology noninvasively and without using extrinsic contrast agents, these methods are ideal for clinical use and for monitoring of chronic cases. In contrast, the other type features high specificity, high spatial resolution, but superficial imaging only and mainly used to image extrinsic fluorescent contrast such as calcium or voltage indicators *ex vivo* or *in vivo*. This type includes multi-photon microscopy, light sheet microscopy, super-resolution microscopy, miniature microscopy[66] and microscopes combined with wave shaping methods such as adaptive optics[67] and wavefront shaping[68] to go deeper. Development of various fluorescent indicators facilitates both observation of activities of mammalian neurons in real time and identification of their synaptic connection[69], and to link their functions with morphology[70]. These tools for studying brain activity have been attractive method as they allow for simultaneous recording of activity from many individual neurons. For optical (e.g., fluorescence) calcium imaging, the calcium signal comes from a group of calcium-sensitive proteins with specific optical absorption,

capable of showing fluorescence changes in intracellular calcium levels in neurons *in vivo*. Figure 8 shows the profile of two-photon brain imaging as an example for this part.
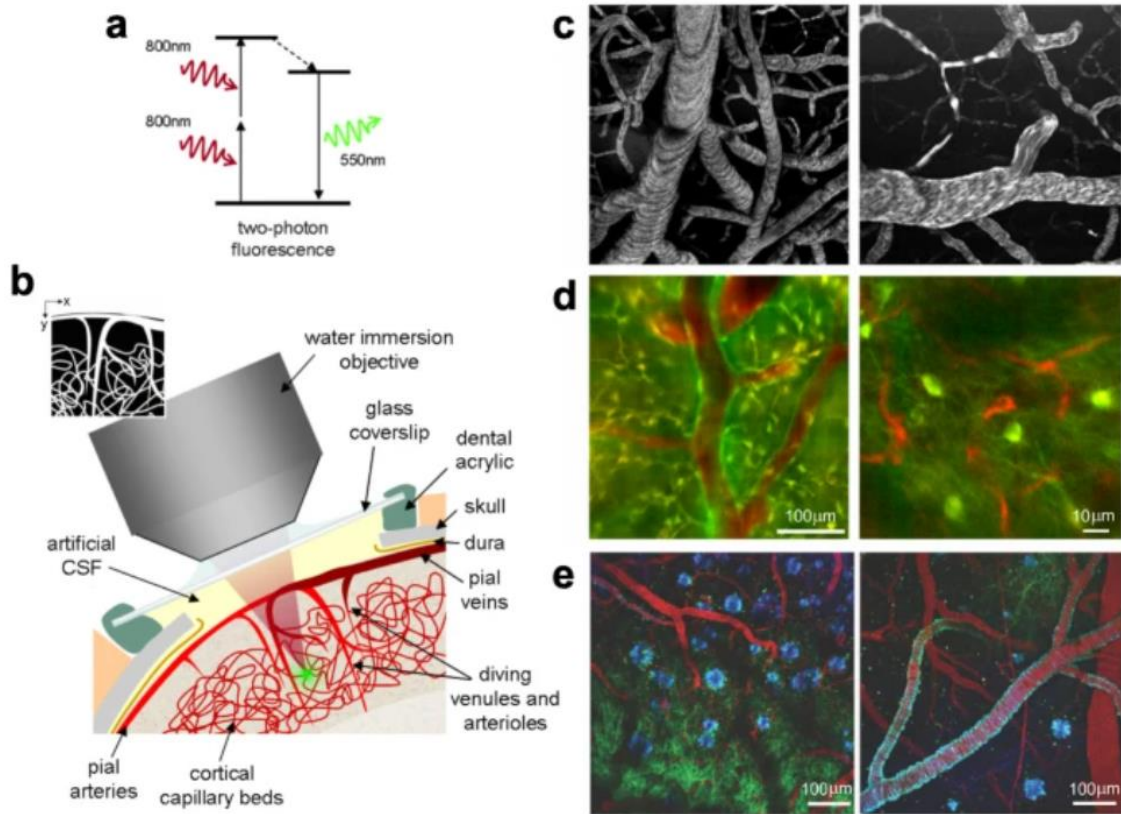
Figure 8 Two-photon microscopy of the brain *in vivo*. (a) Basic principle of generation of two-photon fluorescence. Two low-frequency photons are absorbed almost together, and one high-frequency photon can be generated during decay. (b) Schematic illustration of two-photon imaging with surgery to expose the imaging area to the objective. (c) Two-photon imaging of brain vasculature by using dextran-conjugated fluorescein through intravenous injection. (d) Dual-channel imaging of neural calcium response (green) and blood signals (red). (e) Three-channel imaging of mouse model with Tg2576 APP Alzheimer's disease with amyloid-targeting dye (blue), GFP expressing neurons and dendrites (green) and vasculature (red)[71].

Being able to excite or inhibit specific neural types or neural circuits flexibly, optogenetics has been used in various areas those unimaginable to do with other

19

stimulation methods. The unique target selecting capability make it an ideal tool in neuroscience for deciphering neural circuits transmission in stress[72] and neurodegenerative disorders such as Alzheimer diseases and Parkinson and potential ways to alleviate symptoms[73]. Other potential therapeutic effects include applications in epilepsy[74], memory retrieval[75], hearing[76]/ visual restoration[77], heart disease, pacemaker[78], and cancer[79], etc.

Referring to the concept in Figure 2, neuroscientists are also searching for opportunities to conduct a "closed-loop optogenetics", i.e., electrophysiological recording/ optical imaging/ activity-based readouts guided optogenetic stimulation, as powerful tactics for investigation of neural function in causal and real-time manner[80]. In this scheme, the readouts can be processed online and then used to conditionally modulate on/ off or other parameters of light source, which is both beneficial to neuroscience research to study neural functions and to clinics for seizure detection and prevention. Electrophysiology-optogenetics interfaces such as optrodes[81-83] are conventionally used for simultaneous stimulation and recording. With developments in opsins and optical sensors for neural activity with minimal spectral overlapping so that can work in pair, and with taking full advantage of high spatiotemporal capability of optical techniques, all-optical closed-loop system with online fast and quantitative physiology reading and high-precision optogenetic perturbation has been becoming unprecedented in the neuroscience toolbox and drawing increasing attention. Combination of

GECIs[84, 85] or GEVIs[6, 7, 86] with optogenetics confers possibility of investigating causal link between neural activity and function through all-optical electrophysiology with potential of single-cell-resolution imaging and perturbation[87] within a population of neurons, as shown in Figure 9. Together with photoporation for non-contact gene delivery[88], an ambitious blueprint is all-optical operation of the whole optogenetic process (Figure 10).
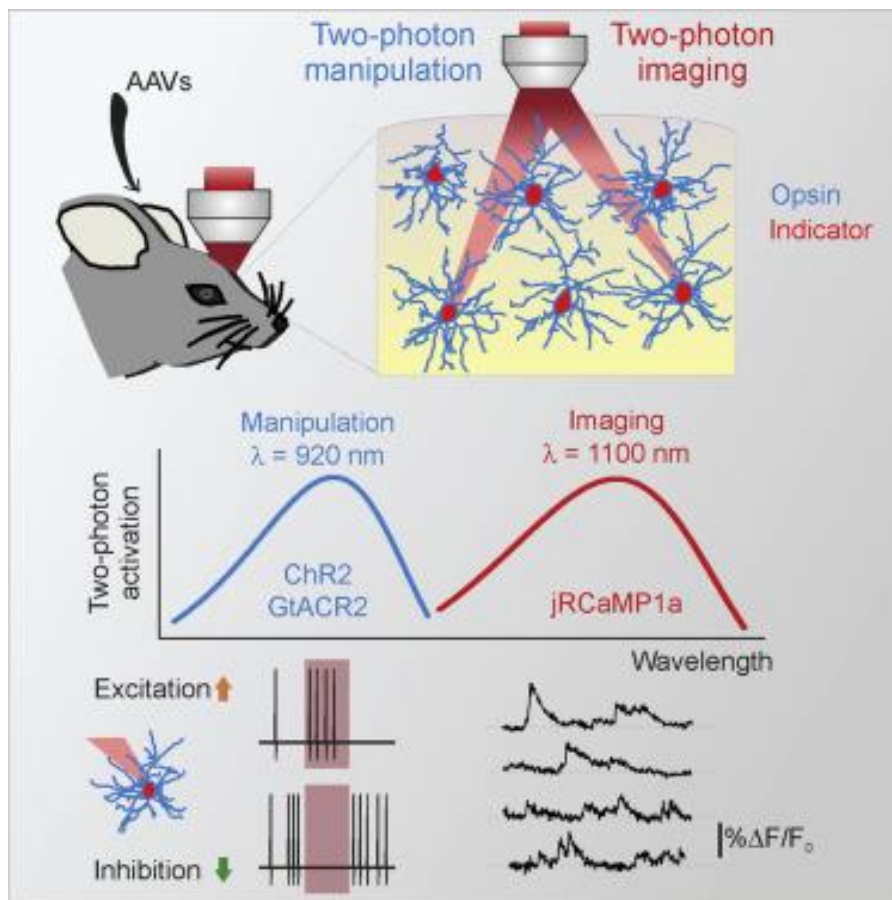
Figure 9 Example of simultaneous all-optical imaging and manipulation[86].
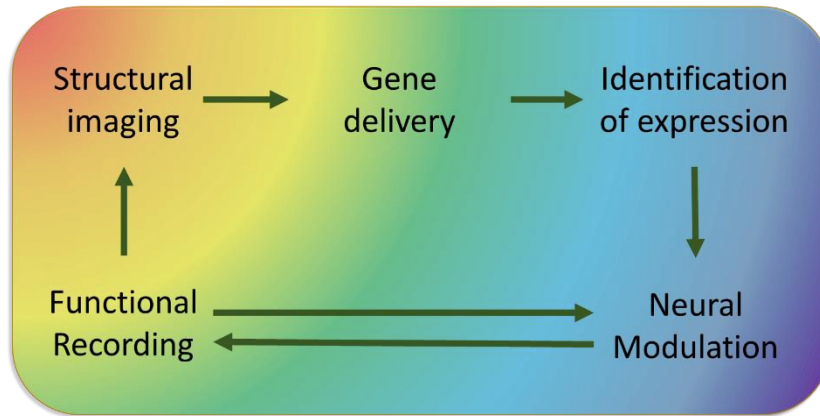
Figure 10 Closed-loop all-optical control including structural imaging guided gene delivery through photoporation, expression analysis, optogenetics along with detection of neural activity.

5. Current challenges in applying optics in neuron science and the theoretical foundations

5.1 Current challenges in optogenetic stimulation

Firstly, it is always desired but still remains a huge challenge to localize light to small volumes deep inside the brain. Fiber-optic based light delivery to some extent narrows the illuminated volume, the spatial resolution achieved is still coarse. And there is a limit of the number of fiber probes that can be inserted. Fine-tuning optogenetic control of small cluster of neurons is thus a difficulty. Secondly, optogenetics stands out of conventional neural modulation methods due to its ability to provide cell-type-specific stimulation. However in practice, to get sufficient power density for stimulation of a volume, light induced heat can affect neurons as well. Commonly used protocols increased the temperature by 0.2-2 °C and suppressed spiking in multiple brain

regions[89], some higher even damage the neuron. In addition, seeing through development of the neural stimulation methods (Part 2 of Chapter 1), we can find that with more and more aspects of neurophysiology goes into control, both biotechnological constraints and invasiveness increase. Optogenetics provides superior spatiotemporal resolution with highest invasiveness. Finally, as mentioned in Part 4 of Chapter 1, the most common used fiber-optic scheme exploits a multimode fiber with 200μm core size. Light power density is highest at the fiber end and reduces dramatically with distancing, which may not stay above the stimulation threshold through the whole illuminated brain region. In general, the utilization rate of light energy is deficient.

The brain tissue is lipid-rich and optically turbid. As illustrated in Figure 11, light output from the fiber end has a natural divergence angle θ, the intensity thus decreases as the distance z to the fiber end increases (Figure 11a)). Considering photons in the wavelength range of 400 to 900nm within which light extinction from scattering is much stronger than that from absorption[90, 91], shorter propagation distance and greater divergence when fiber inserted into brain tissue (Figure 11 b)) is caused majorly by scattering.
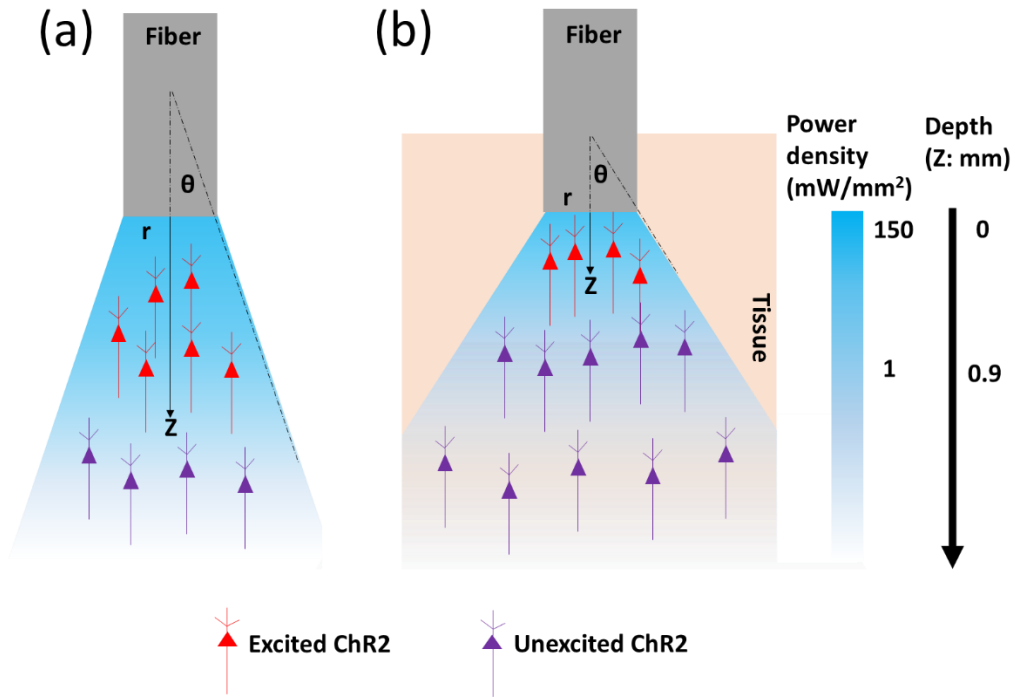
Figure 11 Illustration of light intensity decrease (a) outside the fiber end and (b) from combined effects of geometric divergence and tissue scattering.

Adapting from the Kubelka-Munk model which assume monochromatic illumination, isotropic scattering and no reflection at boundaries[92], light transmission rate (T) in diffuse scattering media can be further simplified assuming no absorption [14]:

$$T = \frac{1}{Sz+1} \quad (1)$$

where S is the scattering coefficient per unit distance and z is the distance to the fiber end.

On the other hand, light exit from the fiber end is normally not collimated and the conical geometry from the fiber output naturally induce intensity decrease with

increasing z regardless of scattering or absorption. The geometric-decreased intensity

with distance z (without tissue scattering and absorption) can be calculated as:

$$\frac{I(z)}{I(z=0)} = \frac{\rho}{(z+\rho)^2} (2)$$

where

$$\rho = r\sqrt{(\frac{n}{NA})^2 - 1} \ (3)$$

in which r is the radius and NA is the numerical aperture of the optical fiber.

The relationship between light intensity and tissue penetration regarding fiber optics is

a combined effect and can be calculated by taking the product of the transmission rate

in considering scattering and absorption only and beam divergence only:

$$\frac{I(z)}{I(z=0)} = \frac{\rho^2}{(Sz+1)(z+\rho)^2} \ (4)$$

A strong intensity gradient with depth can be got from equation (4) when S is equal to

11.2 mm^{-1} and 10.3mm^{-1} for mouse and rat, respectively, as shown in Figure 12. The

intensity drops dramatically to 50% within 100μm of distance beyond the fiber tip, and

10% at about 200 μm. Considering 1mW/mm^2 threshold for ChR2 excitation, superhigh

power density (380mW/mm^2[14]) is needed at the fiber output if a brain volume of

~0.5mm^3 (1.4mm from the fiber tip)is planned to be stimulated to cover a substantial

part of cortex area and induce a specific function.
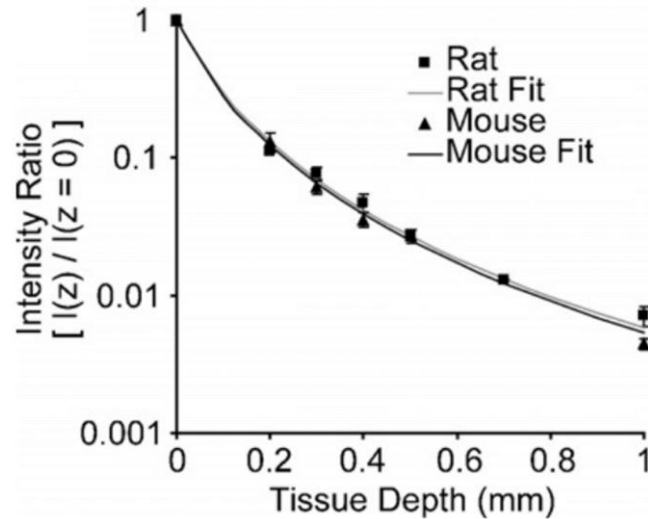
Figure 12 Light intensity at 473nm drops as a function of depth z to the fiber tip[14].

By this delivery scheme, it is only possible to stimulate populations of neurons that are within the illuminating region from the fiber tip and with above threshold intensity. Higher power density is normally necessary for a sufficient volume to be stimulated. Much higher power may produce nonspecific effects. Strong and multi-scattered photons can reach light-sensitive organs such as the retina, which directly elicit neural activity or animal's behavior. Absorbing may also generate heat or even damage the neurons. Local temperature increase, especially at the nontargeted area near the fiber tip, is worth special consideration as subtle changes even without tissue damage may cause significant physiological (0.1-0.4°C[93]) or behavioral(1-4°C[94], [95]) effects. In a typical optogenetic light delivery setup, an optical fiber (200μm, NA=0.37) inserted 0.5mm above a target region with 5mW blue output can provide 4.9mW/mm^2 power density[14] and induce 0.38°C local change in temperature by calculation with ignoring

the mitigating effects from conduction and blood flow over time[61]. By the same calculation method, the temperature increase near the fiber tip (with 380mW/mm^2[14]) can reach 30 ^{o}C.

Opsins are engineered to be more sensitive to red-shifted light and therefore circumvent light attenuation in two aspects[37]. On the one side, most of this method were achieved by developing step-function opsins (SFO), which work with orders of magnitude lower light power; on the other side, red-shifted light suffers less attenuation in biological tissue. But SFOs feature slow kinetics (as shown in Figure 5) and only subtle neural modulation capability[96]. A recent study has demonstrate a totally noninvasive optogenetic process in vivo[97] with millisecond precision, the incident power at the fiber end remains very high due to strong attenuation light inside the brain and we believe there's a long way ahead to get to the bottom of this problem. Considering the most commonly used fiber optics for in vivo optogenetics, methods for improving light delivering efficiency inside the brain is highly desired.

5.2 Current challenges in optical recording of neural activity

Except for EEG and MEG, a few optical methods were developed for wearable recording over the past decades. Such as miniscope, functional near-infrared spectroscopy (fNIRS), and two-photon microscopy (TPM), can provide both structural and functional information from many individual neurons, directly or indirectly,

depending on the tissue properties and the chromophore/dye involved. Excellent contrast and spatiotemporal resolution can be expected, yet with compromised penetration depth due to strong scattering of light in deep tissue [98-103] or high risk of neural damage with densely fired photons. Pure optical approaches are no favored for deep (>200 μm) recording or are limited to volumes <1 mm³ due to the strong light scattering. Given the fact that even the smallest mammals, such as shrews, have a six-layer neocortex of about 0.5mm and that for human 2-4mm, 200μm only touches the first two layers of the cerebral cortex (Figure 13). This is far from getting the integrated information that span all the thickness of the cortex, including specific functions of the deep layers and the connections among different layers with different temporal dynamics. In practice, optical-based brain imaging often requires invasive surgeries to remove the hair, skin, scalp, and even skull to minimize the scattering-induced quality reduction. Going deep is not only about the problem of invasiveness, but a more meaningful gain is also the accurate study of brain function at depth.
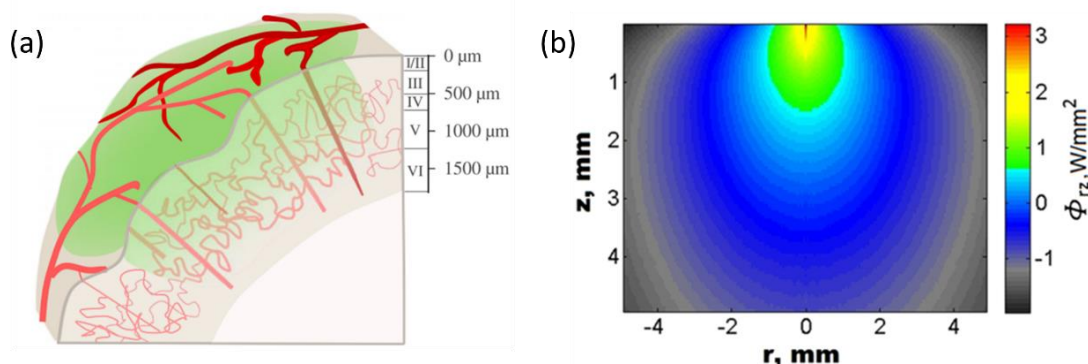
Figure 13 a) Layers of mouse cortex and corresponding depth[104]. b) Light is strongly scattered inside biological tissue during propagation[105]

The theoretical foundation of this problem can be explained as follows. In an ideal imaging system with transparent imaging target, the finest structure in the target that can be imaged will not be smaller than the Abbe diffraction limit[106]. In practice, however, majority of the biological sample in nature are turbid medium, and features heterogeneous distribution of refractive index, which together contribute to scatterring photons through various paths (Figure 14 b)). Some can be directly reflected from the surface of the medium (Specular Reflection); some go into the medium and directly transmit out without interaction with the medium (ballistic photons); some go through one or a few scattering events and then go out from the illuminated surface (Diffuse Reflection); some transmit through the medium after experiencing several scattering events (Diffuse Transmission); others are absorbed after multi-scattering. Number of ballistic photons represents the ability of an incident light beam to pass through tissue and reach the focal plane. Figure 14c) shows that only a small portion of photons can go directly to the focal plane and finally be detected and form a diffraction limited image. These photons are attenuated regarding propagation distance and scattering coefficient of the tissue, and normally can propagate only less than a few hundred micrometers within biological tissues. The majority of photons get multi-scattered and diffused, increase the background noise and degrade the image quality by distorting the ideal wavefront and destroy the ideal diffraction limited focusing spot (Figure 14 d-g)
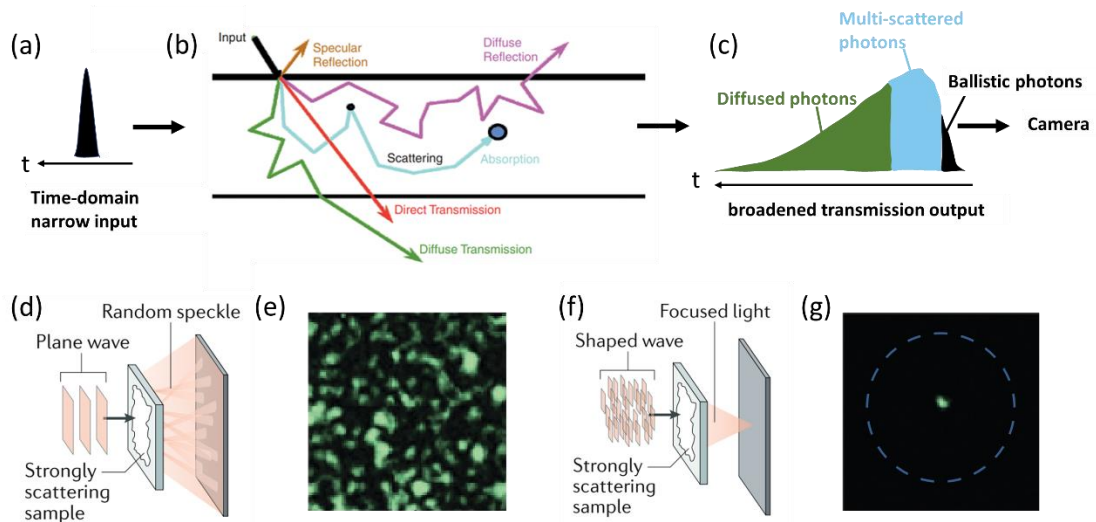
Figure 14 Biological tissue diffuse light temporally and spatially. (a) Temporal profile of an incident light pulse. (b) Visualized paths of photons through tissue[107] showcases scattering induced spatial diffusion of photons. (c) A time-domain broadened pulse after scattering events, adapted from[108]. (d) A plane wave is detected as random speckle after passing through a strong scattering medium, and the speckle profile is shown in (e). (f) A shaped wave plane is reshaped to an optimized/ideal focal point. (d, f) are from [109] and (e, g) are from [68].

With such strong scattering effects, both excitation and emission light can be bended and thus limiting the penetration ability of exciting light and increasing crosstalk of emission light which together degrading image quality at deep tissue. While structure imaging can be achieved by fixing and imaging thin tissue samples, current pure optical imaging methods are facing major challenges to decipher the functional information that requires preservation of physiological condition in large volume and in depth to subcortical regions with cellular/ sub-cellular resolution[109], referring to a mouse cortex layer distribution and corresponding depth (Figure 13).

Efforts have been made transfer from blue to red, which is less scattered, less absorbed and even can penetrate skull[110], through engineering of opsins and indicators for

stimulation and recording, respectively. Such kind of efforts are desired, however, not easy to achieve. Long-wavelength also allow imaging through nonlinear multiphoton mechanism, which allow localized excitation and imaging confined in the nonlinear area with high resolution at depth. Multiphoton microscopy has been the most widely spread modality for preclinical relatively deeper brain imaging with sub-micrometer resolution, compromised imaging depth with acceptable quality remained in superficial brain considering phototoxicity, available fluorophores, spatial resolution and overall cost[111]. These techniques also suffer from low scanning speed. Overall, a technique that can achieve molecular level imaging at depth with high spatiotemporal resolution is highly desired.

Chapter 2   Application of photonic nanojet effect in optogenetics

1. Introduction to photonic nanojet and study overview

Firstly described in 2004, photonic nanojet (PNJ) is a narrow, high-intensity and converged three-dimensional light area generated near the shadow-side surface of an illuminated lossless dielectric microcylinder[112] or microsphere[113]. It maintains a subwavelength beam waist that can be less than the diffraction limit ($\sim\lambda/3$) and focal length over a distance longer than the input wavelength ($\sim2\lambda$) beyond the dielectric cylinder or sphere[114]. It mostly happens when the refractive index contrast (m) between the cylinder/sphere and the background is around 1.7[112, 113], and the diameter is within an intermediate range (λ to 10λ) where neither Rayleigh theory nor geometrical optics is applicable[115]. Microspheres with diameters between 1-10 μm fall into this intermediate range and has been numerically and experimentally observed to generate this phenomenon. Featuring subwavelength-scale and high-intensity focal region, and lower Joule heating as compared to plasmonic resonant systems, PNJ has proved to have broad applications spanning from super-resolution optical microscopy[116], optical trapping[117], nanolithography[118], high-density optical data storage[119], etc.
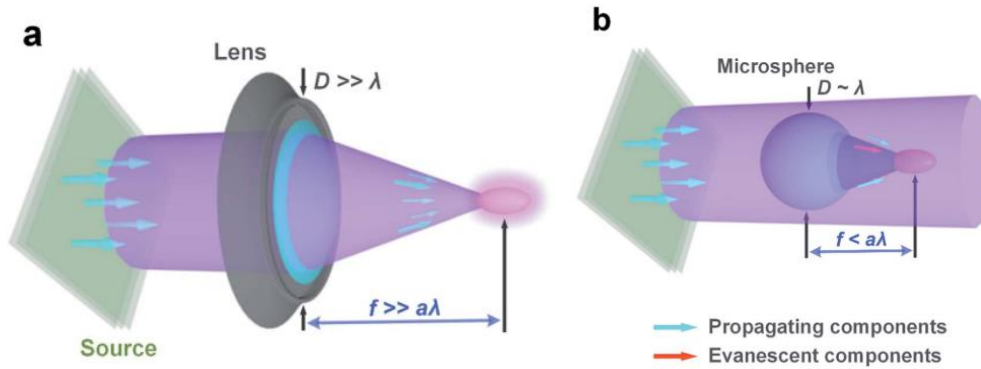
Figure 15 Comparison between (a) macroscale and (b) microscale condensing with plane wave illumination. The focal length in (a) and (b) are far larger and smaller than the wavelength, respectively[120]. λ, the incident wavelength; D, diameter of the lens/ microsphere; f, focal length.

Compared with macroscale condensing by lens, the microsphere generates a nanojet in a short focal length just several times of wavelength beyond the sphere (Figure 15), which is ideal for concentrating light *in vivo*. The study in this thesis for the first time exploiting the photonic nanojet effect for highly localized optogenetics with less input illumination power, which holds potential for optogenetic stimulation at depth, as shown in Figure 16. We first simulate to choose microsphere with most proper size and refractive index that gives the best converging effect in the application context. Then transparent polystyrene (PS) microspheres are mainly used in experiments to demonstrate our idea. Safety issues are then discussed to make practical sense of the proposed method. Compared to upconversion nanoparticle[121] that has shown favorable capability in fighting against tissue scattering, two major advantages exist in current study. One advantage of PS microsphere is its transparency, which is not wavelength-fastidious and superior to upconversion nanoparticles that has to use a

narrow band illumination (which is mostly 980nm, a high-water absorption band). This wavelength transparency is helpful to deeper stimulation where long wavelengths are mostly needed. In addition, applications of current upconversion nanoparticles are impeded by their relatively low quantum yield and thus requires orders of higher incident power than that indeed need for optogenetics. Transparent microspheres, on the contrary, do not have such special requirements.
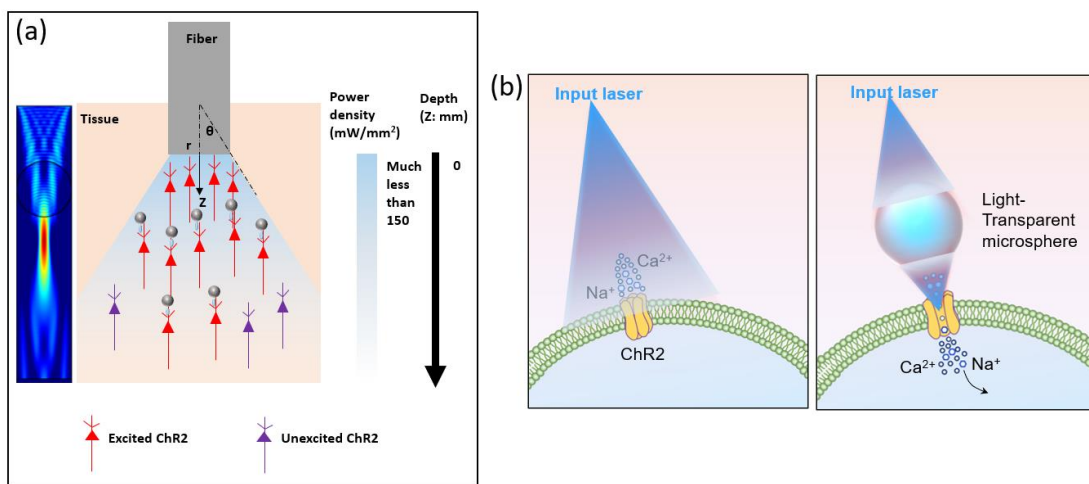
Figure 16 Schematic illustration of microsphere enhanced optogenetics. (a) Photonic nanojet facilitates stimulation of cells locates at deeper region with less incident power. (b) Zoom-in view of light-microsphere-cell interaction, in which light intensity which originally insufficient to interact with a cell can activate a cell with aiding of microsphere focusing. Gray ball: microsphere.

2. Photonics nanojet simulation and measurement

We simulated to compare beam concentration performance of microspheres with several different sizes and refractive indexes (Figure 17) by using FEM method and COMSOL Multiphysics software.
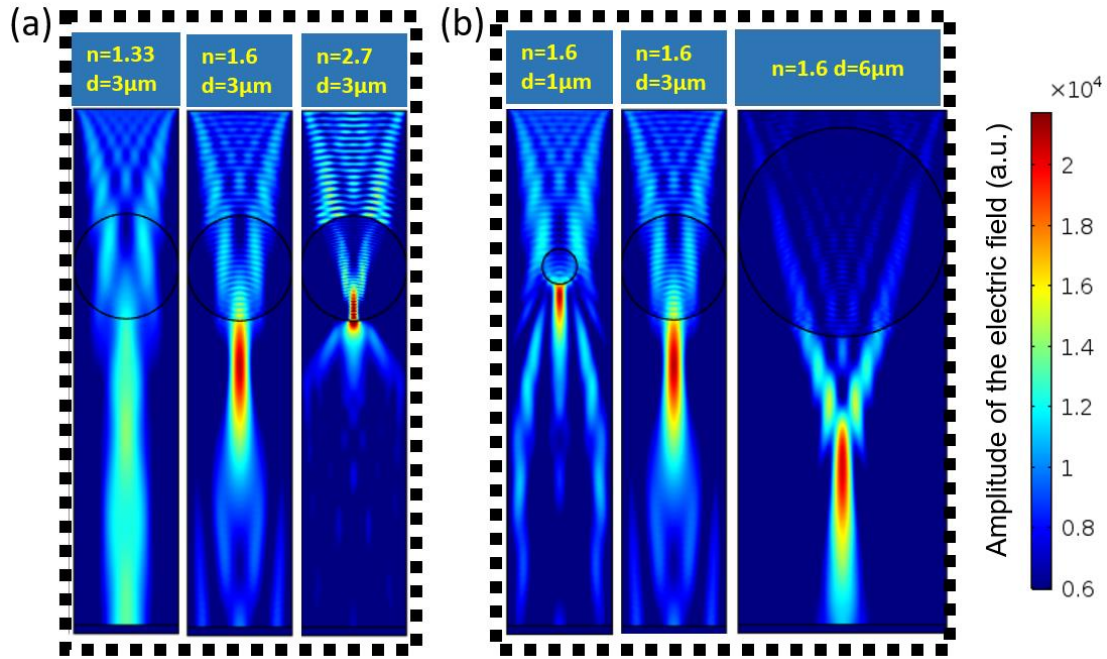
Figure 17 Photonic nanojets generated by dielectric spheres of various sizes and refractive indexes.

Table 3 Quantification of Figure 17. NA, Not applicable.

d=3μm				n=1.6			
n	1.33	1.6	2.7	d(μm)	1	3	6
Waist(nm)	NA	500	400	Waist(nm)	300	480	480
Length(nm)	NA	3000	600	Length(nm)	1400	3000	4600

We chose two materials (n=1.6 for polystyrene, and n=2.7 for titanium dioxide) in the simulation. With a fixing sphere diameter, the focusing region at the shadow side of the sphere become more confined in jet length (600nm) with higher sphere refractive index (2.7), as shown in Figure 17 a) and jets size at full-width-at-half-maximum (FWHM) area are quantified in left part in Table 3. We believe an intermediate jet profile will

perform better in practice. As in this study, spheres are not tightly bounded onto one cell, and the illumination may come from every direction. "looser" and longer jets generated from multi-directions potentially interact more cells and thus should be more efficient than a tightly confined jet that can only interact with one cell each time. Considering current widely available monodispersed and transparent microspheres and the jet profile, we choose polystyrene microspheres (PS) with n=1.6 in further studies. In Figure 17 b), the size effect is investigated. The waist remains around λ, but the jet region becomes longer and further with increasing sphere diameter. For the same consideration about enhancement efficiency in experiments, we choose PS microsphere with 3μm size in further experiments.

On the other side apparently, the electric field amplitude is magnified ~2 times in the concentrated region, the optical intensity is therefore 4 times enhanced. So theoretically ~4 times lower power is needed in microsphere-enhanced optogenetics. The actual enhancement was measured by using fibers. As shown in Figure 18, with using the PS microsphere, the power density is greatly enlarged.
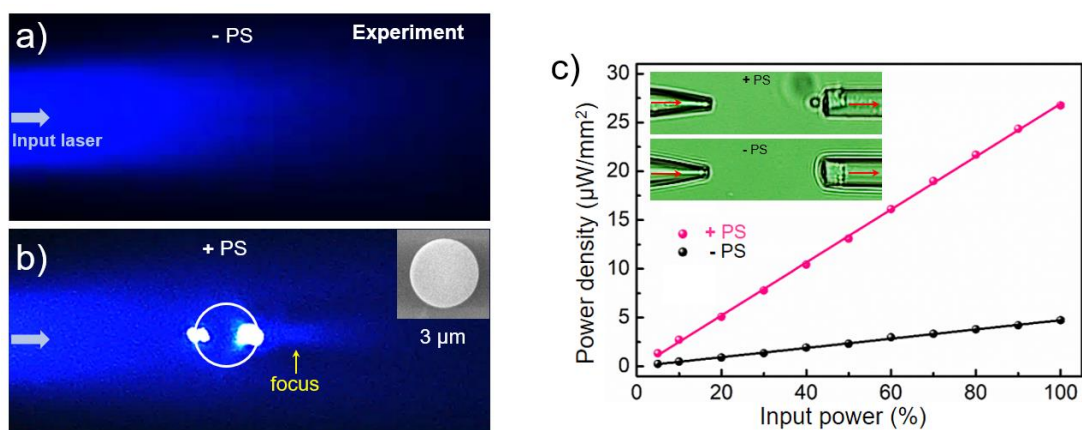
Figure 18 Experimental measurements of power density enhancement with using a PS microsphere.

3. Characterization of microspheres

We characterized commercially available microspheres PS and TiO_2 in DI water, and results are shown in Figure 19. In Figure 19 (a), no peak absorption appears at 488nm or 580nm. According to the peak absorption of ChR2 at 488nm and NpHR at 589nm in neural excitation and inhibition applications respectively, this potentially lessens the possibility of Joule heating by the sphere themselves and guarantee maximum light transmission. Zeta potentials were measured by a Zetasizer Nano Z system (Malvern Instruments Ltd) and microscopy images were got from an Olympus IX73 inverted microscope with an 60X objective (NA=0.7). The near -30mV surface charge of PS indicates mono-dispersion and can be visualized in Figure 19 (c). Comparably, near 0mV surface charge results in slight aggregation in TiO_2 and consistent in the microscopy image in Figure 19 (d) as well. However, even size distribution estimated to be 3um is seen in both.
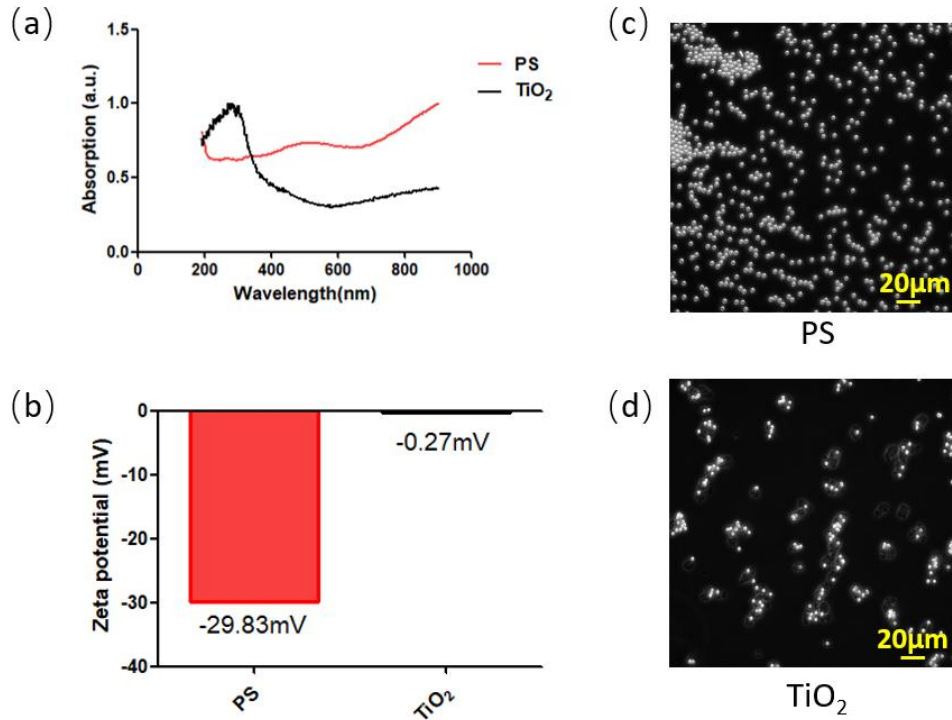
Figure 19 Characterization of Polystyrene (PS) and Titanium Dioxide (TiO$_2$) microspheres distributed in water. (a) Absorption spectra. (b) Zeta potential. (c) and (d) Microscopy images with 60X microscopy.

4. In vitro and ex-vivo demonstration

We first used patch clamp to test the effects of microsphere on cell line and neurons. Figure 20 illustrates the patch clamp configuration. A naked optical fiber tip emitting 488nm light was placed closely to the cell surface to stimulate one single cell. The microsphere enhancement capability was investigated on cells pre- and post- adding microspheres. With microscopic phase imaging and fluorescence imaging (Figure 21, upper row), we firstly confirmed that a cell successfully expressing ChR2-mcherry infusion is under investigation. Microspheres can be clearly visualized in the enlarged view. The relatively large area of the cell body compared to the sphere enables

simultaneous whole-cell electrophysiological recording and microsphere-assisted optogenetic stimulation with minimal potential for electrode-sphere artifacts such as changes in seal or pipette resistance (Figure 21, lower row).
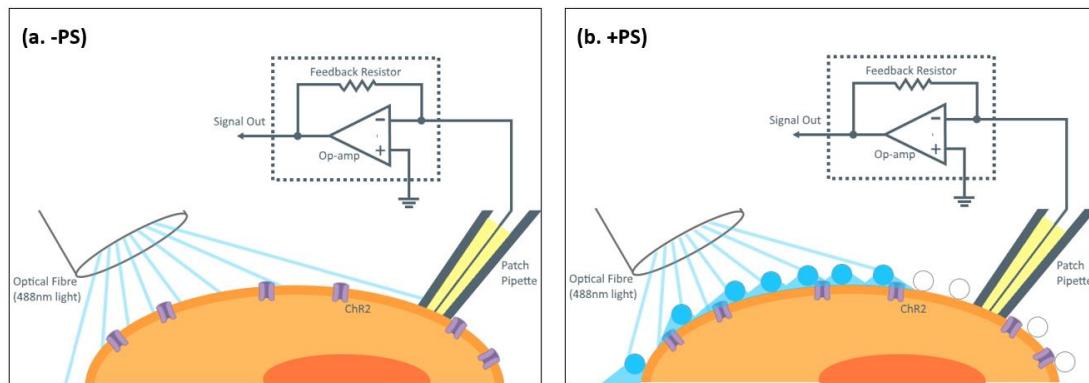
Figure 20 Schematic illustration of patch clamp investigation of optogenetics on ChR2-expressed cells. (a) without and (b) with microspheres.
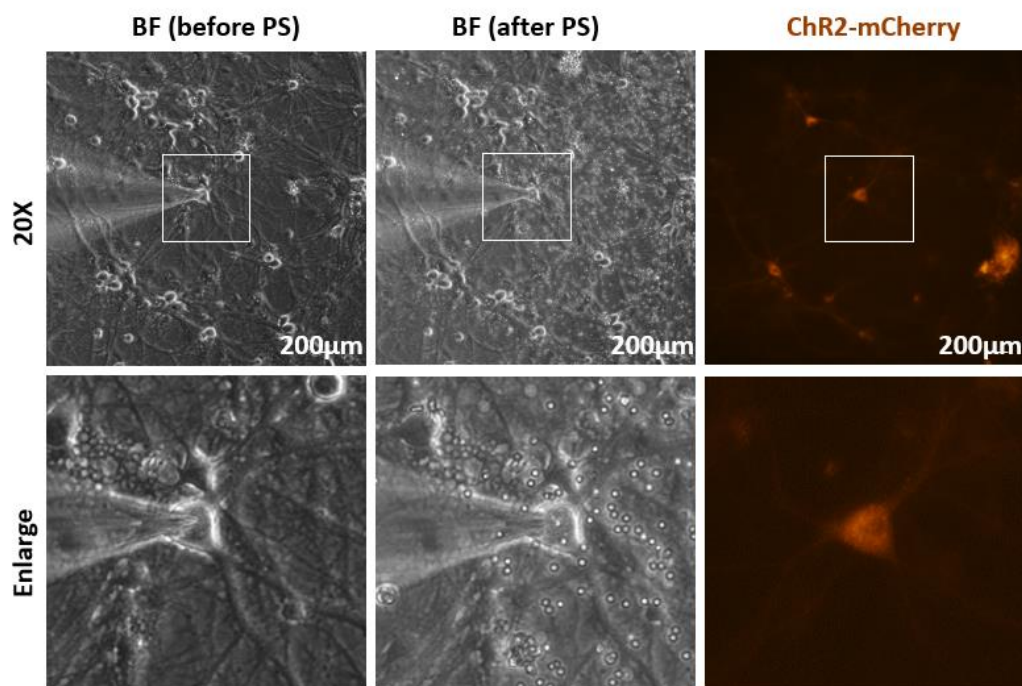
Figure 21 Microscopy visualization of a ChR2-expressed cell under phase imaging and fluorescence imaging before and after adding spheres (PS as example).

Figure 22 shows that stimulation of HEK-293T cell line with 488nm excitation elicits inward currents under voltage clamp condition. In all power conditions from 0.1 to 6.4 mW/mm^2 (Figure 22 a) and b)), the inward currents with adding PS increased faster with increasing stimulation power and current amplitudes were significantly higher than without PS. Maximum current amplitudes of the ChR2 group was observed under 6.4mW/mm^2 excitation power. Whereas PS+ChR2 group increased the maximum current to 1.25 times (~420pA VS ~600pA) at the same power. In another group involving TiO$_2$ microspheres, the ratio of the inward currents between with and without sphere enhancement was larger. At 2.6 mW/mm^2 power condition, ChR2 alone only induce minimum current, while the TiO$_2$+ChR2 group has reached almost its maximum, with a ratio about 4.2 (~100pA VS ~420pA). In both the PS and TiO$_2$ cases, as seen from the inward current profile (Figure 22 a) and b) and in the quantification (Figure 22 c) and d)), the difference between with and without spheres, or the enhancement performance of the spheres was strong at relatively low powers and descends with higher powers. This make sense as cells response to light stimulation with a saturation threshold beyond which no stronger response can be generated. In addition, TiO$_2$ appeared to behave better than PS for application on a single neuron. This consists with its more confined jet region compared with PS as shown in Figure 17, making sure that most of the energy directly interact with the cell membrane where the ion channels locate.
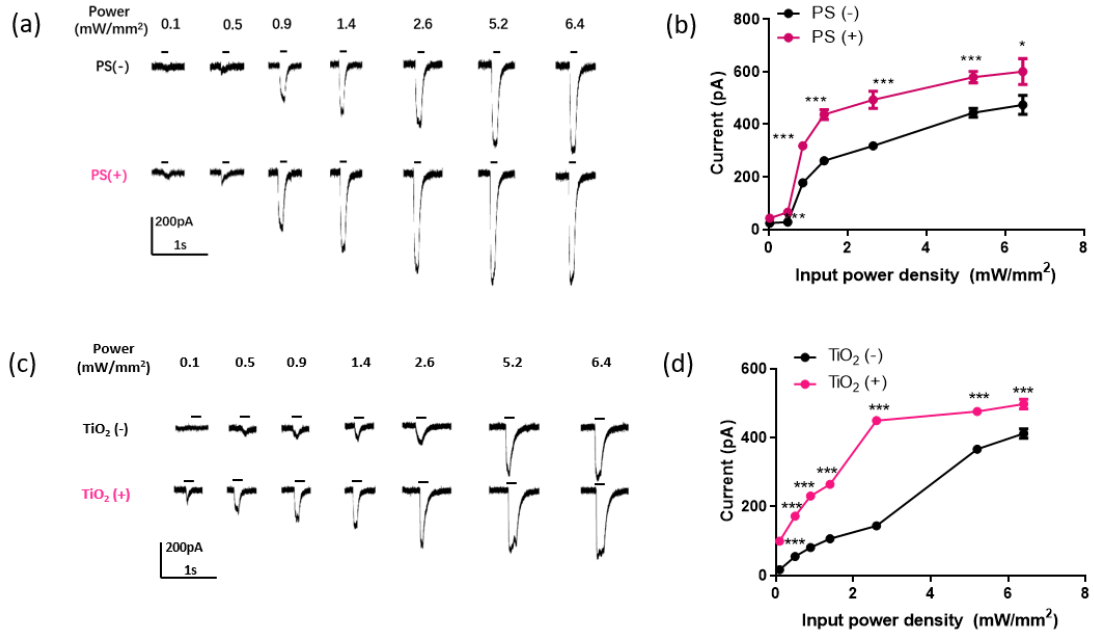
Figure 22 Inward current increases with the increase of excitation light power, and microsphere can elicit higher inward current at a same power. (a) PS enhance 293T cell response to light in a dose dependent manner with quantification in (b). (c) TiO_2 enhance 293T cell response to light in a dose dependent manner with quantification in (d). *p<0.05, **p<0.01, ***p<0.001, unpaired t-test.

After confirming function of the ChR2 protein on 293T cell line as a usual procedure, we next proceed to validation on primary neurons (Figure 23). Both inward currents and action potentials were recorded upon light onset, and microsphere enhancement work similarly. In Figure 23 a) and b), power of PS enhancement keeps being stronger with increasing light dose and a fast-increasing inward current was seen, while the group without PS grows slower. In Figure 23 c), light can stably and repeatably depolarize neurons from their resting potential by about 100mV with 3.1mW/mm^2 power in the no-PS group. The power, in comparison, reduced to less than 2.6mW/mm^2 in the PS group. The successful rate of action potentials by light was significantly enhanced by PS microspheres. (Figure 23 d)).

41
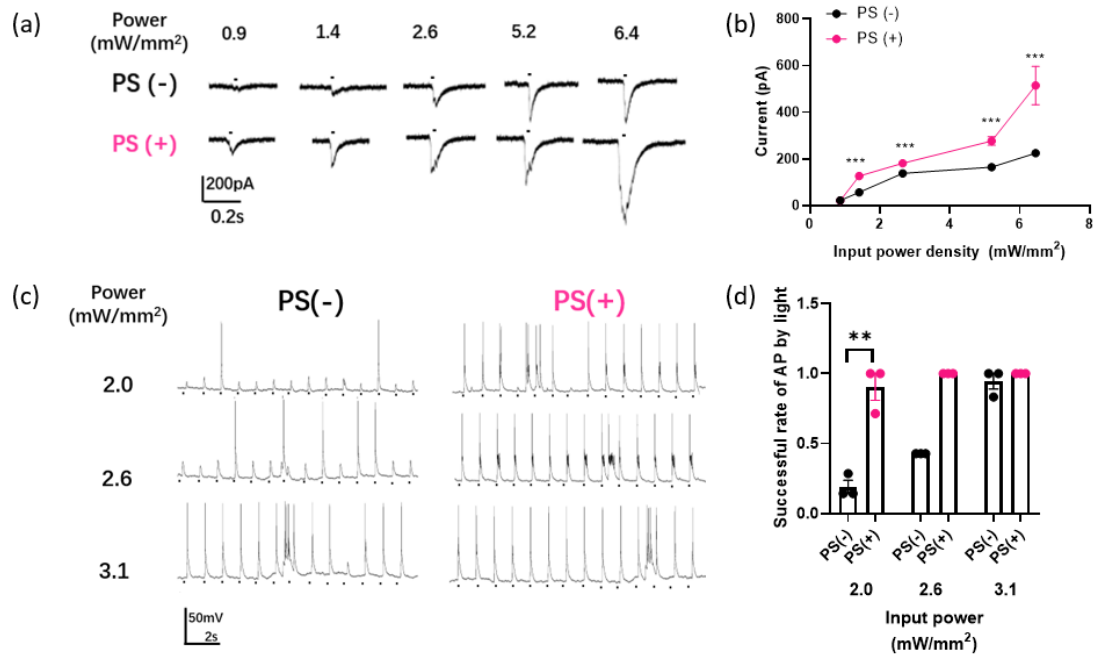
Figure 23 Inward currents and successful rates of neural action potentials increase with the increase of excitation light power, and microspheres facilitates elicit higher neural responses at a same power. (a) PS microspheres enhance neural inward currents upon light stimulation in a dose-dependent manner with quantification in (b). (c) PS microspheres enhance successful rates of neural action potentials by response to light in a dose-dependent manner with quantification in (d). **$p<0.01$, ***$p<0.001$, unpaired t-test.

To test the microsphere-mediated enhanced optogenetics in C57BL/6 mouse line, we performed calcium imaging and Multi-electro-array (MEA) study in acute brain slices of the mice. Before attempting of each experiment, it is important to confirm functional ChR2 proteins are expressed in the excitatory neurons. Acute brain slices were obtained two weeks after natal injection of AAV virus carrying ChR2-mcherry fusion protein with excitatory neuron specific promoter CaMKIIα (pAAV-CaMKIIa-hChR2(H134R)-mCherry). Figure 24 displays large numbers of cellular fluorescence revealing robust expression and natal injection at 0-days post born provide brain-wide expression of the target protein. The fluorescence appears to be majorly localized on the cell membrane,

which has good consistency with previous observation of mCherry expression on neurons.
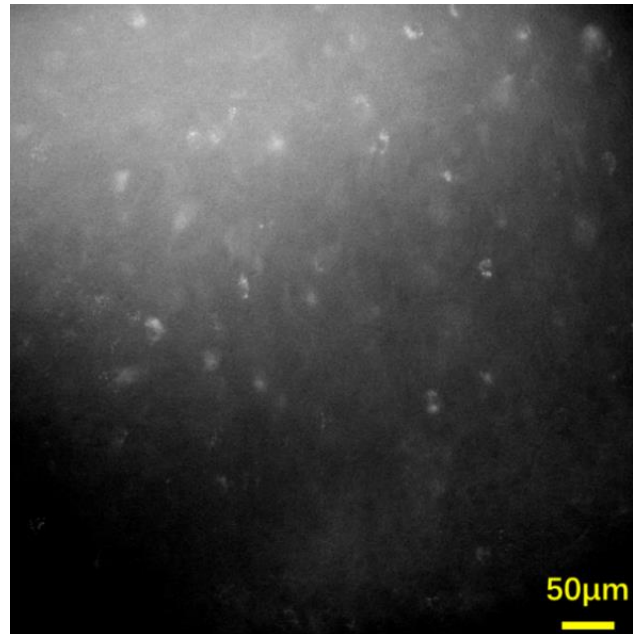
Figure 24 Acute brain slice expressing ChR2-mCherry fusion protein.

MEA allows long-term recordings of local field potentials (LPFs) and extracellular action potentials (EAPs) from populations of neurons at millisecond time scale[17]. The MEA data obtained from *in vivo* or *ex vivo* studies are often very similar, therefore experiments on brain slice can vividly display what happened in real *in vivo* environment. The mice were sacrificed ~two weeks post injection and brain was sliced coronally with 300μm thickness and recorded with a 64-pin MEA system, as shown in Figure 25. The hippocampus region was put on the recording sites, as hippocampal neurons are arranged in the same orientation, the extracellular signals from each neuron don't cancel out but rather add up to give a signal that is strong enough to be recorded

by a nearby field electrode.
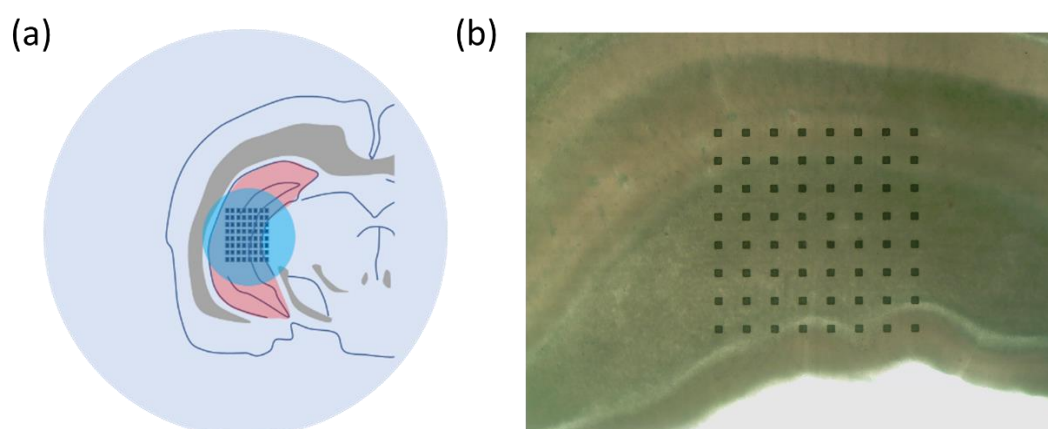
Figure 25 Hippocampus recording in an acute brain slice of coronal section with a 64-pin MEA system. (a) Illustration of positions of electrodes (black squares), brain slice (with hippocampus shown in pink), and blue light illumination (blue area in the center). (b) A microscopic image to confirm that the hippocampus region placed on the electrodes in experiment with a 4X objective.

Figure 26 shows the averaged raw data of spikes elicited with 3x10s blue light illumination (1Hz, 10ms). ChR2 alone (upper row in Figure 26) induced spikes has minimum change with increasing power. While in the ChR2+ PS group elicited significant difference (see quantification in Figure 27) upon very low power stimulation (2.2mW/mm^2). The difference keeps growing till 3.5mW/mm^2 light power. This result is consistent with the patch data (Figure 22) that PS can significantly enhance neuron response to light. While the difference seen with no light input but just after adding PS microspheres may probably be due to the surface charges of the microsphere which influence the neural activities.
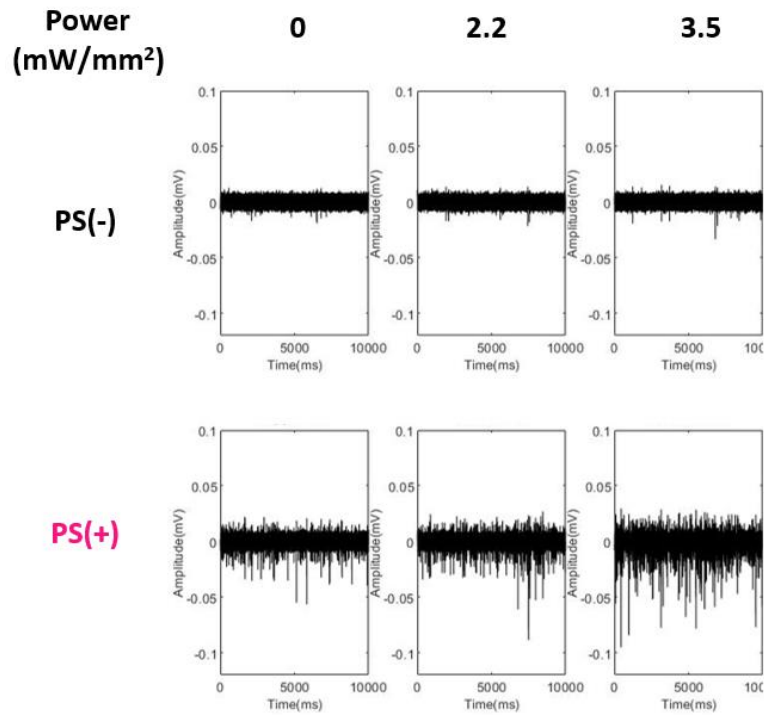
Figure 26 Raw data of MEA signals from one representative channel upon light stimulation on ChR2 expressed brain slice. Upper row: Increasing light power before adding PS. Lower row: Increasing light power after adding PS.
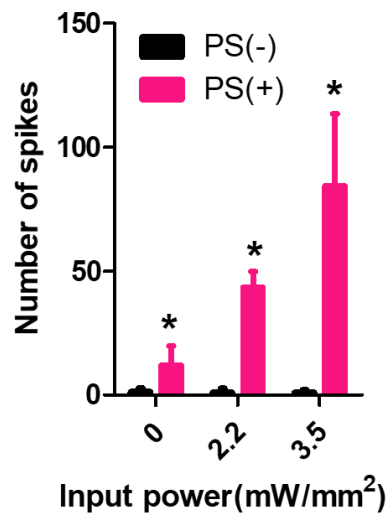
Figure 27 Number of spikes quantified from Figure 26. The bar chart represents means ± SD of brain slice stimulated by light with increasing power and compared from three independent recordings. n = 3, *p < 0.05, unpaired 2-tailed t tests.

These spikes represent changes in the extracellular field due to ion flux (Na^+, Ca^{2+}…) in the local environment[3, 17]. Among all the ions, calcium act as the second messenger that convert electrical signals into chemical activity in addition to control cell excitability and therefore is the mostly studied among all ions in the central nervous system[122]. Calcium signals have been the surrogates for direct measurement of single-cell action potentials since all cells use changes in intracellular calcium concentration to regulate cell signaling events. Neurons especially, with their elaborate dendritic and axonal structures, both localized and widespread calcium signals have been captured. Neural action potential is associated with influx of calcium ions. Exocytosis of neurotransmitter triggered by calcium influx in presynaptic terminals starts neural communication. The intracellular concentration in resting state is less than 100nM, while rises around 10 to 100 times higher when excited and generating action potentials[123]. Monitoring calcium ion flow can facilitate the monitoring of action potential firing, which can be achieved at single neuron resolution by using optical measurements comparing to electrode recording.

Therefore, we next investigated whether the microsphere-assisted enhancement works through magnified calcium influx on acute brain slice by microscopic imaging of an intracellular calcium indicator which has peak absorption far away from the peak absorption of ChR2. Compared to field recording in MEA, calcium imaging can have single-cell resolution, thus no need to confine the imaging region to hippocampus area.

Imaging was conducted 2 minutes pre- and 5 minutes post-shot with an inverted fluorescence microscope before and after adding PS spheres in the same field of view, so that calcium response of the same cells can be tracked, and that microsphere concentration should not be a factor that may lead the results. The experimental setup and procedural observation were shown in Figure 28, and results are shown in Figure 29 and quantified in Figure 30. 50 cells were analyzed in each case and an "imaging only" group was set to exclude unexpected excitation by the imaging beam because of spectral overlap between the imaging wavelength with the absorption spectrum of ChR2. It is obvious in Figure 29 that this overlap induced excitation can be ignored. And PS has greatly increased neuron calcium response at $3.5mW/mm^2$ light power. Compared to the MEA results, $2.2mW/mm^2$ did not elicit detectable neuron response indicated by fluorescence change. These may result from superimposed factors including sensitivity of the camera, sensitivity of the calcium-sensing dye, and one-shot stimulation instead of multi-pulse stimulation in MEA, fluctuations of power density among experiments, etc.
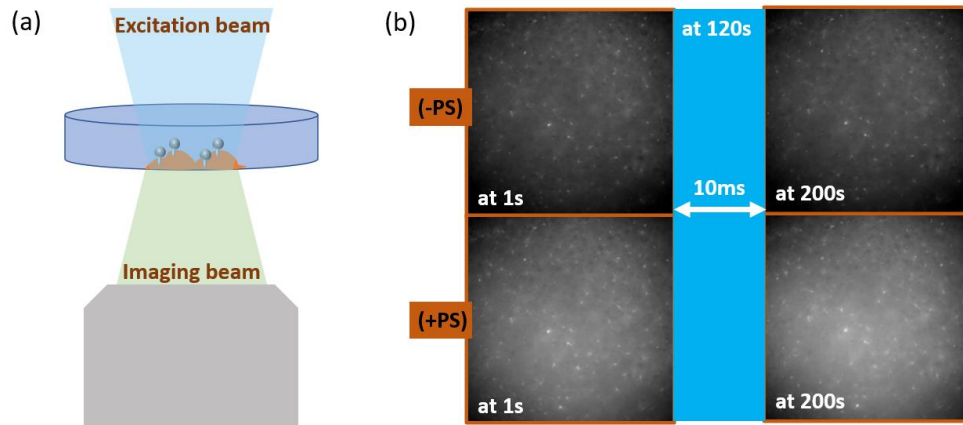
Figure 28 (a) Setup for calcium imaging of microsphere-enhanced optogenetics. (b) Procedural observation of fluorescence increasing after light stimulation during experiment in the PS group.
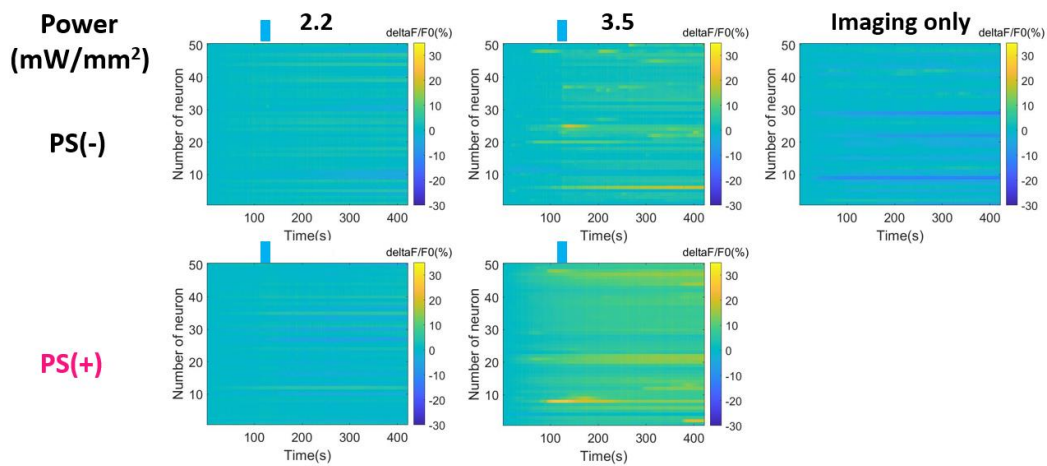
Figure 29 Addition of PS microspheres evokes greater calcium influx.
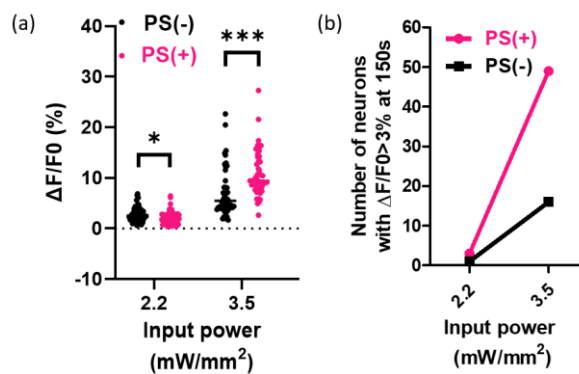
Figure 30 Quantification of Figure 29. (a) Maximum fluorescence change of each cell. (b) Excited neurons those reach $\Delta F/F0>3\%$ at 150s are counted.

5. In vivo demonstration

In addition to give major cellular and molecular level readouts, behavior study is necessary to gather macroscale information about the enhancement performance. Mixture of virus and microsphere (1:1) was injected into the primary motor (M1) region of C57BL/6 mice in the right hemisphere (AP: 0.25mm, ML: -1.5mm, DV: -1.0mm), and optogenetics was performed three weeks after till ChR2 protein is fully expressed (Figure 31a)). Zoom-in view in the blue circle shows the hypothesis that at deeper region beyond the fiber tip where the optical power density becomes very low and ChR2 protein cannot be excited. With addition of the PS microsphere, these membrane proteins got larger chance to be stimulated by enhanced optical power density near the sphere.
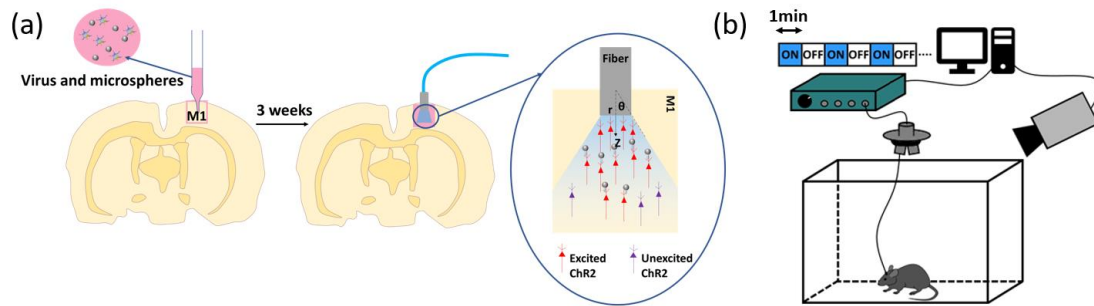
Figure 31 Scheme for *in vivo* experiments. (a) Mice aged 8 weeks were injected with a mixture of viruses and microspheres in the primary motor area (M1) in the cerebral cortex, and fiber was inserted two weeks after injection. Mice were treated with light stimulation (15Hz, 10ms, 1min on and 1min off) with increasing power one more week after. (b) Illustration of the setup used for in vivo recording.

In the experiment, we used light pulse with 15Hz repetition rate and 10ms pulse width

for stimulation. The stimuli keep one minute on and then one minute off to allow the subject to recover to natural state (Figure 31b)). Upon starting the next round stimulation, the power is increased so that we expect to get a dose dependent response to know the intensity threshold for driving a specific behaviour in ChR2 alone group and in ChR2+PS group. The results are shown in Figure 32. Compared with mice injected with ChR2 only, photo-stimulation of mice injected with ChR2+PS reliably evoked increases in average speed, speed change, and total distance travelled (Figure 32 b-d)). At low stimulation intensity ($1.4 \ mW/mm^2$), the animal behavior showed little difference to that of light-OFF state for the ChR2-only group, while ChR2+PS induced significant difference in animal behavior at the same photo-stimulation power. The evoked rotating speed was much higher and total distance travelled were much longer compared to light-OFF state in the ChR2+PS group than in the ChR2-only group at the same condition. At a relatively high stimulation intensity ($5.6 \ mW/mm^2$), the difference got even more significant, indicating much more enhanced optogenetic light-triggered behavior. Representative rotating trajectory upon light stimulation is shown in Figure 32 a). In this in vivo study, effects of PS kept positive when incident power going higher, which seems to contradictory to the i*n vitro* and *ex vivo* studies. However, this is acceptable due to various parameters those may affect the in vivo output such as opsin expressing level, opsin quality and animal condition, etc.
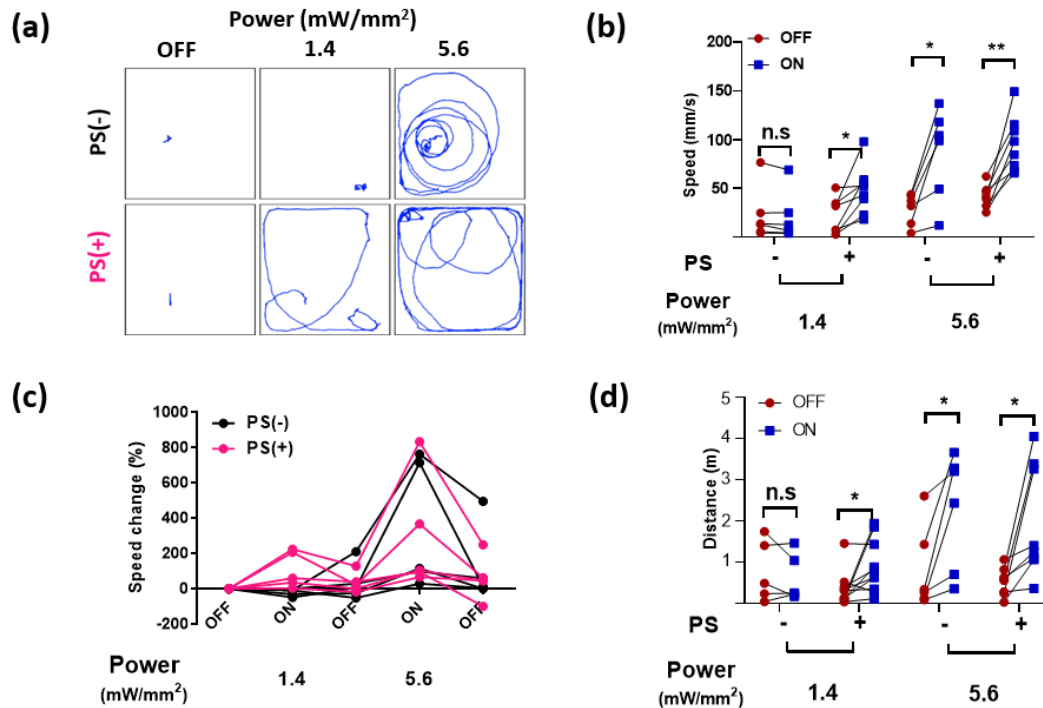
Figure 32 PS can enhance the optogenetic locomotion. (a) Trajectory analysis of mice in three different doses of stimuli. Mice in the ChR2-alone group (PS (-)) were drove to rotate with higher stimulus dose (5.6 mW/mm^2) while only 1.4 mW/mm^2 power is needed in the PS+ ChR2 (PS(+)) group. (b)-(d) Optogenetics evoke increase in (b) speed (c) speed change and (d) distance travelled in light-ON state compared to light-OFF period, the changes are larger in the ChR2+PS groups and groups with higher stimulation powers than those of the ChR2-alone groups and groups with lower stimulation power. n=4 in each group, *p < 0.05, **p < 0.01, unpaired 2-tailed t tests.

In addition to intracellular calcium signal in acute brain slice, the *in vivo* stimulation effect can be evaluated in single-cell manner by testing expression of c-Fos, a marker protein that is induced expressing immediately-early upon receiving external stimulation and that is widely used as a functional and anatomical mapping tool to identify successfully activated neurons in response to stimuli[124]. Minimum light power was used in this experiment (only 5%, 15Hz, 10ms, 1min on) and mice was then sacrificed 60min later to allow maximum expression of c-Fos protein. The ChR2-positive areas are identified by mCherry fluorescence (red) and colocalization (yellow)

of c-Fos (green) and mCherry was then counted, with representative images shown in

Figure 33 and quantification shown in Figure 34. The ChR2 alone group has averaged

c-Fos positive cells counted about one while that of ChR2+PS groups has more than

two per unit region, the difference is significant enough as shown in Figure 34.
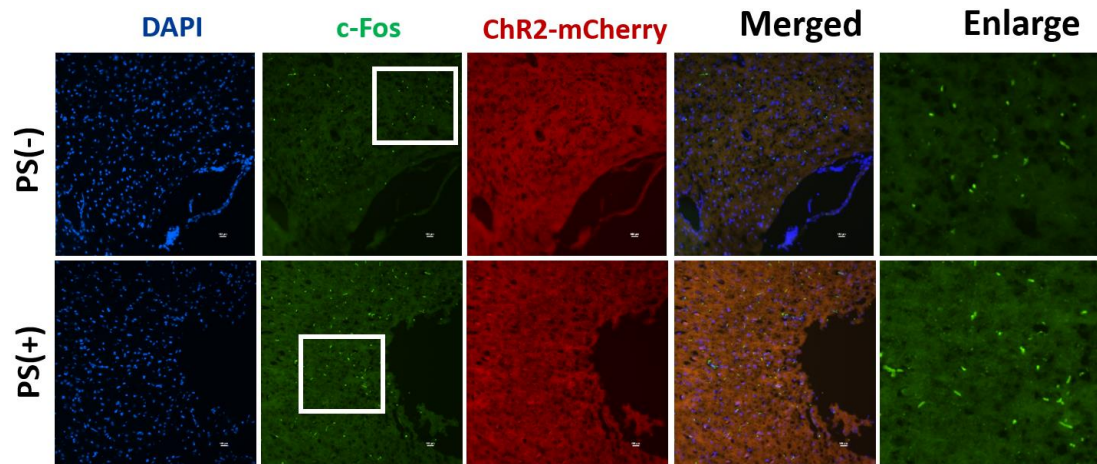
Figure 33 Representative images of M1 mouse cortex treated with light stimulation without or with PS microspheres, stained for c-Fos expression. The mice were sacrificed 60 min after stimulation with minimum power (5%, 15Hz, 10ms) for 1 minute, and their brains slices were imaged for DAPI (blue), mCherry (red), and c-Fos (green) expression.
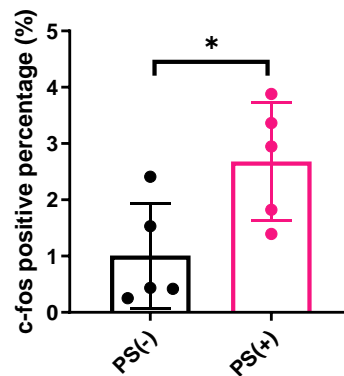
Figure 34 Quantification of Figure 33. The bar chart represents means ± SD percentages of c-Fos-positive cells per unit area. n= 5, *p < 0.05.

6. Methodology in this chapter

Simulation

FEM method and COMSOL Multiphysics software is used. All spheres are assumed dielectric and transparent. Refractive index of tissues are very near to ambient solution environment[125] and thus approximated to indices of water. Microspheres of different diameters (d) are embedded in the water environment (refractive index of water: n=1.33). 488nm plane wave incidences from the upper port, and a perfectly matched layer (PML) at the bottom for terminating the electromagnetic field. Scattering boundary conditions are used for all the external boundaries and continuous boundary conditions are default for all the internal boundaries. The simulation is conducted by solving:

$$\nabla \times \mu_r^{-1}(\nabla \times E) \cdot k_0^2 \left(\epsilon_r - \frac{j\sigma}{\omega \epsilon_0} \right) E = 0 \ (6)$$

Animal

C57BL/6J mice of eight weeks old were used for *ex vivo* and *in vivo* experiments. Standard housing condition with 12h light/dark alternation and food and water available ad libitum are provided for holding animal. All procedures regarding animal operation were conducted with strictly following the guidelines of the Department of Health - Animals (Control of Experiments) of the Hong Kong S.A.R. government.

Cell culture

Primary neurons were obtained at the 16th embryonic day from the mouse embryonic cortices as described in[126]. Cortices were firstly immersed and sectioned in ice-cold Neurobasal medium and then incubated for 15min in 0.25% trypsin-EDTA in a water bath at 37°C. Cells were then collected by centrifuging and washing with Neurobasal medium with 10% FBS, 0.25% L-Glutamine and 1% Penicillin-Streptomycin once. Cells were then centrifuged again and resuspended in medium followed by mechanically triturated with a pipette and then statically settled to get the supernatant removed. Then cells are resuspended in medium further containing 2% B27 serum-free supplement and seeded in 35mm dishes containing poly-L-lysine (PPL)-coated coverslips at 5×10^5 cells per dish. The medium was changed 24h after to Neurobasal + 0.25% L-Glutamine + 2% B27 +1% Penicillin-Streptomycin and half rechanged every 72h.

293T cell line were purchased from ATCC. Cells were incubated in a humidified incubator maintained at 37°C with 5% CO_2. The culturing medium consisted of Dulbecco's Modified Eagle Medium (DMEM), 10% fetal bovine serum, 100 μg/mL streptomycin, and 100 units/mL penicillin.

Viral transduction

High-tilter viruses (pAAV-CaMKIIa-hChR2(H134R-mCherry)) were obtained

commercially and stored at -80°C prior to use. ChR2 gene sequence was fused with that of the fluorescent reporter mCherry We used a CaMKIIα promoter to preferentially transduce only excitatory neurons. Virus diluted 1:100 in PBS was added to primary neuron cultures at DIV7 at room temperature. For each dish with 5×10^5 cell density, 10^{10} genome copies were directly added into the cell medium. Then the plates were gently shaken and put back into incubator for 3-5 days under monitoring of fluorescence and cell condition. Successful transduction with bright fluorescence were used in further experiments.

Patch Clamp

7 days after virus transduction, patch clamp was used to record the light-evoked membrane potentials on primary cortical neurons. Borosilicate-made glass patch pipettes (Vitrex, Modulohm A/S, Herlev) were pulled by using a micropipette puller (P-97, Sutter Instrument Co.) and filled with pipette solution to have a resistance of 5–7MΩ. Current clamp was applied for measuring membrane potential and voltage clamp was applied for measuring inward current. Cells were bathed in their original medium and can be visualized in 3D by phase contrast microscopy. Good transduction was confirmed by fluorescence imaging. The pipettes filling solution contains 1 mM MgCl$_2$, 138 mM KCl, 10 mM HEPES ,10 mM NaCl, and D-mannitol compensated for osm 290 (pH 7.2). Digidata 1440B (Axon Instruments) and amplifier (Axopatch-700A, Axon Instruments) together with pClamp Version 9 software were used for data recording The

data were analyzed by using Clampfit 10.0.

Intracerebroventricular viral injection

Viral injection to the intracerebroventricular region of the neonatal mouse brain was conducted for brain-wide transduction and at the same time guarantee more active brain slice can be used in further experiments. This method has been described in detail previously[127]. Briefly, P0 pups were first anesthetized on ice and then injected virus by using a 10μL syringe with a 32G needle within 6 hours of their birth. The head of the pups were gently wiped with a cotton swab soaked in 70% ethanol before injection. 3/5 of the distance from the eye to the lambda suture was identified as the injection point. Then 1μL thawed virus aliquot was loaded into the injection syringe and the pup was laid on its side having its head directly under the syringe. The syringe needle was perpendicular inserted to the pup skull to a depth of 3mm. Both injection and withdraw of needle were done slowly to make sure virus aliquots do not leak out. Pups were then labeled and put near a warm source to allow recover of body temperature and then put back to their mother cage. Condition of the pups were monitored every day in the first few days after injection.

Preparing of acute brain slices

Two weeks after intracerebroventricular viral injection, mice are deeply anesthetized and decapitated. Brains were taken out quickly and sliced in ice-cold and gas-bubbled

artificial cerebral spinal fluid (ACSF) containing 124 mM NaCl, 10 mM Glucose, 3 mM KCl, 26 m $NaHCO_3$, 2 mM $CaCl_2$, 1.25 mM NaH_2PO_4/H_2O, and 2 mM $MgSO_4/7H_2O$. The gas constitutes with 95% O_2 and 5% CO_2 to maintain a pH of 7.4 in ACSF. Coronial sections with 300μm thickness were sliced by using a vibrating microtome (Leica VT1200S) and recovered in 37ºC gas bubbled ACSF for 1h before experiments.

MEA recording

Individual brain slice was placed into the MED probe (MED64, Alpha MED Scientific Inc, Japan). Slice anchors and mesh netting were used to keep slice adhere to the electrodes. Position of the hippocampus area was adjusted under the microscope. Bathing solution for recording was frequently refreshed manually by gas-bubbled rACSF containing 3 mM KCl ,124 mM NaCl, 10 mM Glucose, 26 m $NaHCO_3$, 1.25 mM NaH_2PO_4/H_2O, 1 mM $MgSO_4/7H_2O$ and 2 mM $CaCl_2$. After system noise checking suggested by the MED system user manual, spontaneous neuronal spikes were recorded with low cut frequency at 100Hz and high cut frequency at 10000Hz. Slice was kept not moving during recording to make sure signals recorded in a specific channel before and after adding microsphere were from the same brain area. Light was coming down from the top of the probe dish. Three traces were recorded under each light intensity. Number of spikes was counted with threshold of ±0.01mV.

Calcium imaging

The prepared acute brain slices were stained with a fluorescent calcium indicator X-Rhod-1, AM (X-14210, Invitrogen) at 4μM final concentration in the rACSF with gas bubbling at room temperature. Stained slice was then placed into a confocal dish for microscopy. The stimulation and imaging system consists of an inverted fluorescence microscope (IX73, Olympus) with Cy3 filter and a sCMOS camera ((ORCA- Flash4.0 LT Plus C114400-42U30, Hamamatsu)) and 488nm light shed from top down. Slices were imaged for 2 minutes before stimulation as baseline and then stimulated with only one shot (10ms) blue pulse and imaged for another more 5 minutes. The stimulation period (10ms) was not imaged. During imaging, a perfusion pump continuously pumped fresh bathing solution (gas-bubbled rACSF) to keep the brain slice in its best condition.

Stereotaxic injection and fiber insertion

C57BL/6 mice were anesthetized with xylazine (10 mg/kg) and ketamine (100mg/kg) in PBS. Hairs above the operation location were shaved and scalp was scissored allowing exposure of the skull. Mice was then fixed onto the stereotaxic apparatus and a hole was drilled on the skull with coordinates AP 0.25 mm, ML -1.5 mm, DV -1.0 mm for M1. Mixture of 500nL pAAV-CaMKIIa-hChR2(H134R-mCherry virus aliquots and 500nL microsphere suspension was injected at 0.1μL/min speed, followed by

keeping the injection pipette 10-minutes at the injection site. The pipette was then withdrawn slowly with another 5-minute pause halfway. The sergery site was then disinfected and sutured followed by returning the mice to their housing room. Three weeks later, the mice were anesthetized and underwent surgery again to insert fiber ceramic ferrule at the same coordinate. The fiber was fixed with dental cement pulled by small screws on the skull. Wide-field behavioral recordings were conducted one week after fiber insertion.

Optogenetic manipulations

Ex vivo optogenetic processes including MEA recording and calcium imaging relied on a 488nm laser providing various repetition rates, pulse widths, and powers. Open field behavior testing was conducted within a $40cm \times 40cm \times 50cm$ field box. 10min habituation were allowed to reduce the acclimation noise. Behavioral parameters including trajectory, speed, and total distance were extracted using a commercial software Toxtrac. Power density during experiments with beam spot size of ~1mm diameter used can be measured by a power meter (Thorlabs) and then calculated.

Immunohistochemical fluorescent staining

60min after light treatment, mice were heart perfused with PBS followed by 4% paraformaldehyde (PFA) (cat. no. P1110, Solarbio) in PBS. Brain slices with $10\mu m$ thickness were dissected with the paraffin method. Slices were then blocked by

blocking buffer (10% normal goat serum + 0.3% Triton in PBS +5% BSA) for 2h in room temperature. Followed by incubating 16-18h using primary antibody (c-Fos (9F6) Rabbit mAb, Cell Signaling Technology) solution diluted (1:500) in blocking buffer in 4°C environment. After gently and completely washing with PBS, slices were incubated with secondary antibodies (Goat anti-Rabbit IgG (H+L) Cross-Adsorbed Secondary Antibody, Alexa Fluor 488, Invitrogen) diluted (1:1000) in the blocking buffer for 2h at room temperature, followed by washing, drying, mounted on glass slides with adding Prolong Diamond Antifade Mountant with DAPI drop wise, coverslip capping over and then imaging. Samples were imaged by using an upright confocal microscope registered in the UBSN facilities in The Hong Kong Polytechnic University. Cells showing colocalized c-Fos signals (green) and mCherry (red) were counted manually in five unit areas.

7. Summary and discussion

In this study, we use polystyrene microsphere as an example and demonstrated that transparent microsphere can significantly enhance the optogenetic response at relatively low light stimulation power by exploiting its natural photonic nanojet effect. This systematic study was conducted in multiple facets from cellular level to animal level. The results have given us confident that optogenetics could be much more efficient to generate the same response with much less power with assistant of transparent microspheres, and thus the fiber insertion can be potentially unnecessary,

and it is possible to go very deeply into the brain with microsphere plus long-propagating red/ near-infrared-light stimulation, or even neural modulation at a distance (remote control). Looking back to the general background of this thesis, less invasive and less harmful generally means more widely applicable.

Safety is a prime and imperative concern. The central nervous system has an elaborated scheme to isolate foreign bodies through a combination of chemical and cellular pathways via the immune system. The causes of neuroinflammatory response can be numerous, the mechanical mismatch can be one of the major factors. Hence, general approaches to combat or "trick" the immune system is to modify the interfacial materials to make them more closely match the tissue mechanics and therefore can follow the motions of the brain[128]. Figure 35 A) shows the Young's modulus of tissue and various materials used in neuron-probe interfaces. Hydrogel has closest mechanical property to tissue and is the most compatible. PS microsphere has Young's modulus estimated to be 3200-3400 MPa[129], which is much stiffer than tissue. However, another approach suggests that stiffer materials still can be used when their dimensions are small enough in the (sub)cellular scale (1-10μm) to enable mechanical compliance, as shown in Figure 35 B). To minimize inflammatory responses in extended applications, surface coatings such as hydrogel coating or PEG coating is expected to help efficiently reduce inflammatory factors.
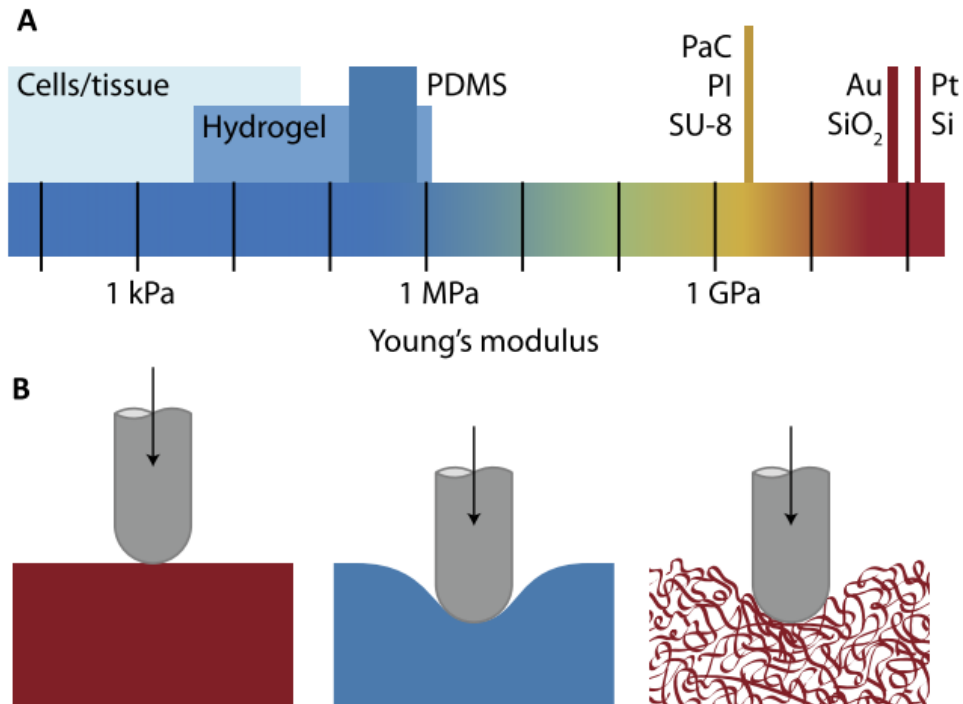
Figure 35 Mechanical mismatch between soft neural tissue and common probe materials. (A) Young's modulus of biological tissue and some common materials. (B) Schematic illustration of the mechanical compliance of stiff inorganic materials (Si, metals, oxides; left), compare to elastomers like poly (dimethylsiloxane) (PDMS; middle); Materials with high modulus and are nominally rigid can be made compliant by minimizing the critical dimensions (right)[128].

Shining light into brain tissue may also result in temperature rise, which will induce altering of cell function thorough affecting enzymatic reactions, molecular conformational changes and molecular interactions[130]. Photothermal neural stimulation[131] is also a possible way for modulating neurons. In our study, to ensure neuron excitation is purely induced by light stimulation through light-gated ChR2 channel, but not by heat through other thermal-sensitive channels, the temperature increasement during laser radiation was measured by a thermal meter, and we find no obvious temperature increasement was induced (Figure 36). This demonstrates that

adding PS microspheres will not subvert the gene-coded specificity as thermo-based stimulation mostly have non-genetic and non-localized heat provided selectivity.
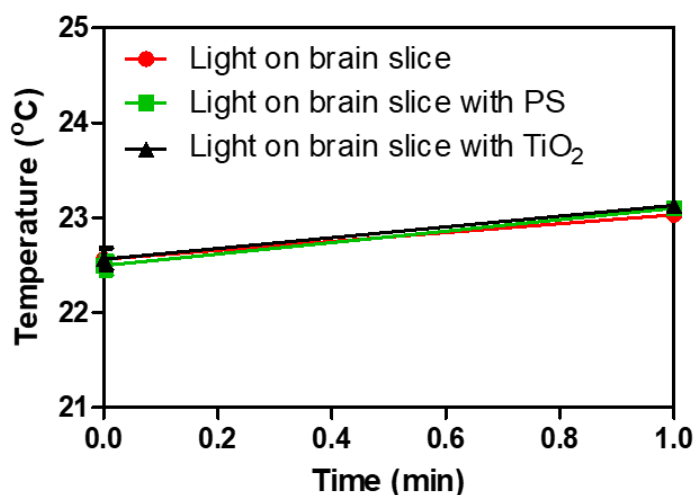
Figure 36 Temperature increases during 488nm laser radiation on an acute brain slice (15Hz, 10ms, 1min).

Particle diffusion inside biological tissue is another issue that may affect the penetration and dispersion in tissue and thus the overall efficiency. The diffusion profile is mostly believed to be affected by particle size, surface charge, material, particle-cell interaction, etc., and finally determines the particle concentration on each cell. Experiments and analysis in this study are based on a certain fixed concentration of spheres to see their general influence and have not gone into too much detail in this regards. Although results have shown significant positive effect of adding PS microsphere on optogenetic efficiency in this study, the microsphere parameters can be further improved regarding this application. This could be another topic in the future.

Chapter 3   Photoacoustic recording of neural activity during naturalistic behavior

1.   Photoacoustic imaging is less affected by tissue optical scattering

Since scattering plays such an important role in biological optical processes, instead of trying hard to remove multi-scattered photons like strategy used in nonlinear multiphoton microscopies for brain imaging, there exists another method which tries to take advantage of the scattering effects during incident propagation and reduce their negative influence the way back to the detector. Such a method introduces the photoacoustic effect though detection the ultrasound signal generated by absorbed photons. Figure 37 illustrates the photoacoustic working principle. Briefly, incident light is multi-scattered in the tissue and absorbed by an absorber. The local temperature rises steeply in time and generates ultrasonic wave during propagating under the thermal confinement and pressure confinement conditions. The generated ultrasonic wave then can be detected by ultrasonic transducers and finally reconstructed to an image of this absorber. On the one side, multiple scattering events increase the rates that photons hit absorbers, be absorbed and then generate ultrasound waves. On the other side, as soft tissue is relatively transparent to ultrasound which is ~1000 times less scattered in tissue than light[132, 133], the imaging resolution and imaging depth can be significantly improved compared to pure optical ways. Looking back to Figure 14 b, c) in Chapter 1, the photon usage rate can be much more improved if multi-

scattered and absorbed photons can be utilized as well. Combining with appropriate absorbers which can represent physiological processes, photoacoustic brain imaging provides a smart way of recording neural activities deep in the brain.
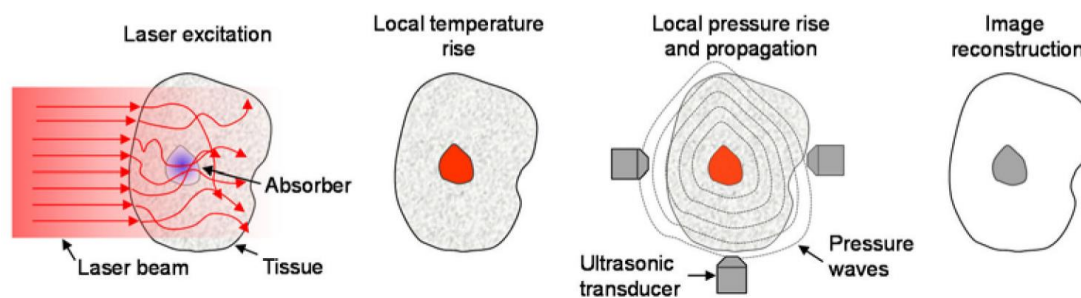
Figure 37 Principle of photoacoustic tomography (PAT)[134].

2. Photoacoustic brain imaging

Photoacoustic imaging (PAI) based on the photoacoustic effect, harnesses optical absorption generated contrast and acoustic signal detection and avails benefits of optical resolution and acoustic penetration (Figure 37). PAI overcomes the optical diffusion limit ultrasonically and combines rich contrast of optical interrogations with high resolution and clinically relevant depth of penetration. PA is sensitive to blood hemoglobin absorption and becomes effective to monitor blood oxygenation by measuring oxygen saturation (sO_2)[135]. In addition, other intrinsic absorbers such as lipid[136], melanin[137], water[138], and a variety of exogenous contrast agents have been explored in PAI for anatomical, functional, and molecular kinetics imaging. As a result, PA has attracted tremendous interests in the past two decades and demonstrated

great potential in various preclinical and clinical applications.

PA systems have been developed in various scales for brain imaging (Figure 38). Compared to confocal fluorescence microscope, optical resolution photoacoustic microscope (OR-PAM) has realized diffraction-limited imaging at about 1mm, with higher optical sensitivity compared to two-photon microscopes. Acoustic resolution microscope (AR-PAM), in which the acoustic focal point is smaller than the size of the optical focal point, normally have tens-of-micros lateral resolution and millimeters of imaging depth. Photoacoustic computed tomography (PACT) has the largest penetration depth of several centimeters, with hundreds-of-microns lateral resolution. Since early demonstration in the year around 2000, dramatic system development in this field has been emerging. Various PAI systems have been used in brain imaging. The first demonstration of noninvasive PA for brain imaging was in 2003[139], in which the structure of the whole brain and functional imaging of cortex upon stimulation of a rat brain was imaged transdermally and transcranially. This study has encouraged tremendous studies of the brain using this modality and various structural[140], functional[141], and molecular imaging[142] in different depths and resolutions have been demonstrated from then on.
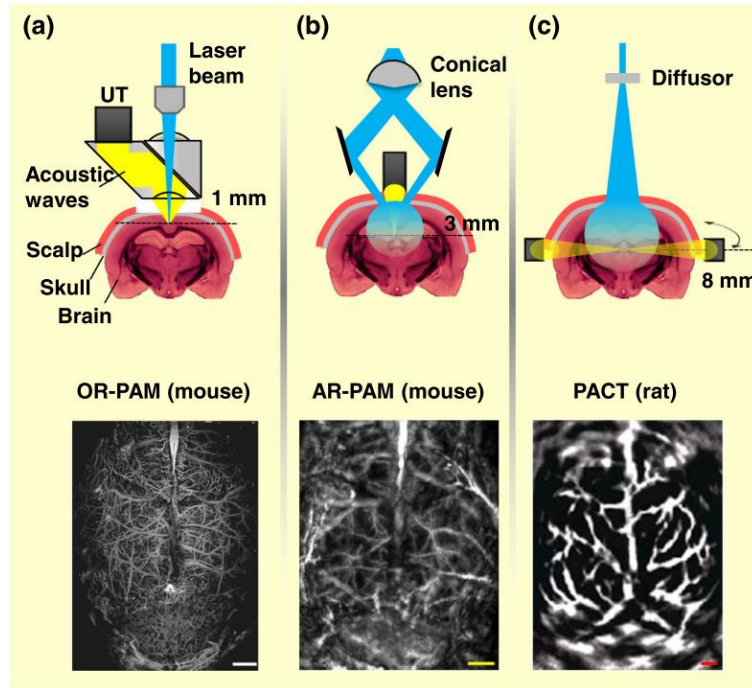
Figure 38 Photoacoustic brain imaging in multiple scales. (a) Imaging of mouse cortical vasculature with the skull intact but the scalp removed by using optical-resolution photoacoustic microscopy (OR-PAM). (~3μm lateral resolution and <1mm penetration depth) (b) Acoustic-resolution photoacoustic microscopy (AR-PAM) of cortical vasculature with both scalp and skull intact in a living adult mouse. (~70μm lateral resolution and ~3mm penetration depth) (c) Photoacoustic computed tomography (PACT) of the cortical vasculature with both the scalp and skull intact in a living rat. (200μm lateral resolution and 8mm penetration depth) [143]

The above systems are mainly for anesthetized and fixed animals. As mentioned in Chapter 1, most of the current imaging studies were conducted in a head-fixed condition and in anesthetization, which not only give the animal additional emotional stress, but also are incompatible with free explorations in real experimental environments. *In vivo* neuroscience studies always desire a miniaturized or wearable device, worn on animal's head, to improve the accessibility, throughput, and quality of brain-imaging studies in freely behaving mice. Such a wearable device should have minimal impact on the animal's head and pose least effect on the animals' normal behavior. Imaging capability

of non-invasiveness, deep brain penetration, wearability, high spatiotemporal resolution, and neuronal functionality, which can be applied to freely moving animals, is urgently needed and still not yet available.
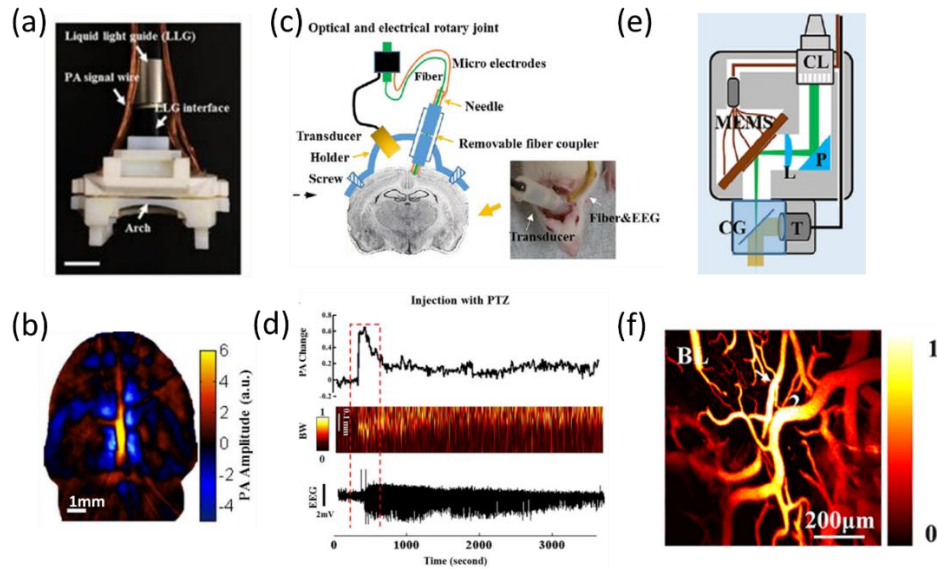
Figure 39 Wearable and head-mounted PAI devices. (a) PACT and (b)whole brain imaging in depth[144]. (c) PA A-line and integrated with an electrode for (d) simultaneous recording of blood flow and electrophysiology[145]. (e) OR-PAM and (f) brain vascular imaging[146].

Based on these considerations, a series of wearable and head-mounted PAI devices has been developed. Tang et al[144] developed a wearable PACT that can do 3D imaging in behaving rats with ~200um lateral resolution for both structure and functional imaging. Figure 39 a) shows a photograph of the 3D wearable PAT probe. The cerebral blood vessels can be clearly imaged (Figure 39 b)). By visual flash stimulation, PA signals from different areas of the brain can be readily recorded. Despite the wearable PACT system, wearable A-line[145] (Figure 39 c) and d)) and wearable OR-PAM[146] (Figure 39 e) and f)) has also been developed for brain study in behaving rats. In the

wearable A-line configuration, micro-electrodes were placed in parallel to the optical fiber and integrated into a needle guide, an ultrasound transducer is placed confocally with the needle tip. An optical and electrical rotary joint was used facilitating free moving of the animal. Blood flow in a single capillary and neuron activities around were recorded simultaneously by PA recording and electrode recording both in anesthesia and during moving. This system has lateral resolution ranging from 0.9μm to 8.8 μm as a function of the distance between the fiber tip and the capillary. The authors further promoted from this invasive A-line recording to imaging of a larger field of view and developed less invasive and wearable OR-PAM device, as shown in Figure 39 e) and f)). In this study, a micro-electromechanical-system (MEMS) was used for optical scanning and a 10MHz flat ultrasound transducer was used for signal receiving. The final probe weight was 8g and FOV of 1.2mm×1.2mm with 2.25μm lateral resolution and 105μm axial resolution, respectively. Cerebral vascular morphology and hemodynamics were monitored both during ischemia and reperfusion on a freely moving rat.

However, it must be noted that accurate interpretation of neural activity from hemodynamic changes requires profound understanding of quantitative relationships between cerebral blood signal and neural activity, which is currently in bridging. The blood oxygenation change is also influenced by other physiological activities and may not be sensitive enough to sub-millisecond-resolved individual neural activity. Thus,

blood oxygenation monitoring alone cannot picture comprehensive information about neural activities.

Recently, it has been shown that it is possible to use genetically encoded calcium indicators (GECIs) to generate PA signals. GECIs can be expressed in designated neural structures, cell populations, cellular organelles, and can provide signals down to the level of action potentials of a single neuron. In addition, it provides the possibility for long-time repeated imaging, such as several days or even up to years. Fluorescence of the protein would be inhibited with the absence of calcium ion. These appealing features have attracted more and more use in photoacoustic imaging [147, 148]. Combination with gene transfection empowers PA imaging the capability to simultaneously obtain vital neuronal functionalities (e.g., blood hemodynamics, oxygenation, and calcium induced action potentials). For example, iGECI[149], a newly developed fluorescence and photoacoustic dual-modality molecule for neural calcium imaging, has enabled simultaneous monitoring of neuronal and hemodynamic processes in the mouse brain through an intact skull.

Therefore, PA imaging can be a good platform for developing a noninvasive deep-penetrating wearable neural imaging device for freely moving animals and monitoring blood oxygenation and neural calcium response simultaneously. Combination of photoacoustic technique with gene transfection technique will take brain and neural study to a new era. In this ongoing study, we aim to develop a wearable and head-

mounted miniaturized photoacoustic microscope (w-PAM) for real-time photoacoustic imaging of blood oxygenation and calcium signal with single cell resolution on freely moving small animals. For this device, the excitation light is tightly focused to an optical diffraction limited area, and the PA signal generated is then detected by a confocally aligned focused ultrasound transducer. w-PAM can provide ~μm-scale focal spot with single-cell resolution, as well as more sensitive signal acquisition compared to unfocused photoacoustic tomography (PAT) systems. The proposed w-PAM would be capable of recording neural activities in the superficial and deep cortex with high spatiotemporal resolution and would be convenient for brain functional imaging of free moving animals. The success of this study will provide a new device for research in neuroscience and give a more comprehensive and unprecedented understanding of neural activities in more detailed scales in freely behaving animals from both blood-oxygenation and calcium-influx points of view.

3. Experimental design and results

A wearable head-mounted PAM system, as illustrated in Figure 40, is designed for real-time neural activities visualization with affordable cost and performance. As shown in Figure 40, the major components of the head-mounted scope include a multiwavelength pulsed laser source as the light source; a small aperture GRIN lens as the optical converging lens; a hollow focused transducer for better alignment of the optical and acoustical foci to ensure imaging sensitivity; a MEMS mirror for fast scanning of the

light; and a plastic yet solid printed holder to fix all these components and mount the miniaturized probe onto the mouse head. The MEMS mirror can scan through an area in a range of ±6° tilt angle about both x- and y-axes by varying the voltage applied, with a scanning speed of up to 500 rad/s and a response time of less than 100 μs. The imaging system aims to have a lateral resolution of 3 μm, an imaging depth of up to 1 mm, and an imaging area of about 1mm^2 considering the scanning speed of the MEMS mirror. All components are easily assembled into a 3D-printed plastic case specially designed by using the SOLIDWORKS software. The case is designed with reference to the size of a mouse head and fixed onto mouse's skull, like a semi-permanent hat. The rest of the system would be attached only during the experiment. This whole system (zoom-in picture) weights 8g and the size is comparable to a coin, as shown in Figure 41.
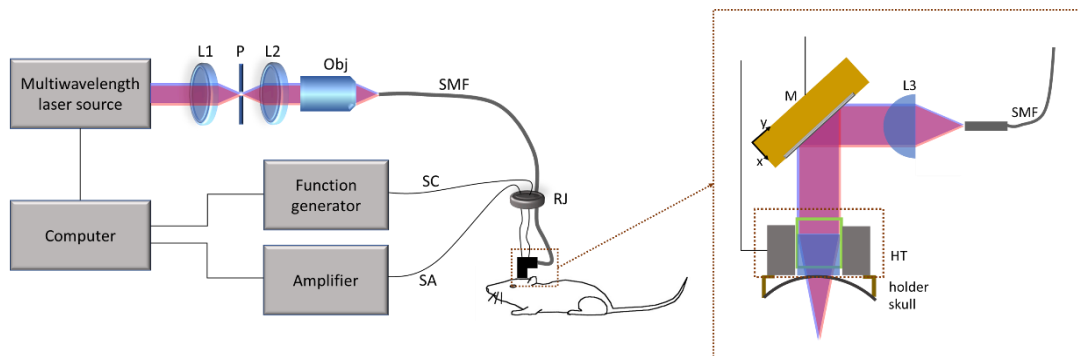
Figure 40 Schematic illustration of the proposed wearable PAM system. L1, L2, L3, lens; P: pinhole; Obj: objective; SMF: single mode fiber; SC: scanning control; SA: signal acquisition; RJ: rotary joint; M: MEMS Mirror; HT: hollow transducer.

Figure 41 Size and weight of the wearable system.

In parallel, we tested the brain calcium response to stimulation via a calcium sensitive dye (X-Rhod-1), by electrical stimulation of brain slice and in vivo recording of the calcium influx during head movement. As shown in Figure 42 and Figure 43, the fluorescence amplitude of the dye can change according to external stimulation or internal brain activity and can well capture the cellular calcium influxes happened in the brain. This has laid a solid foundation for future experiments by exploiting signal from this dye as representative of brain responses.
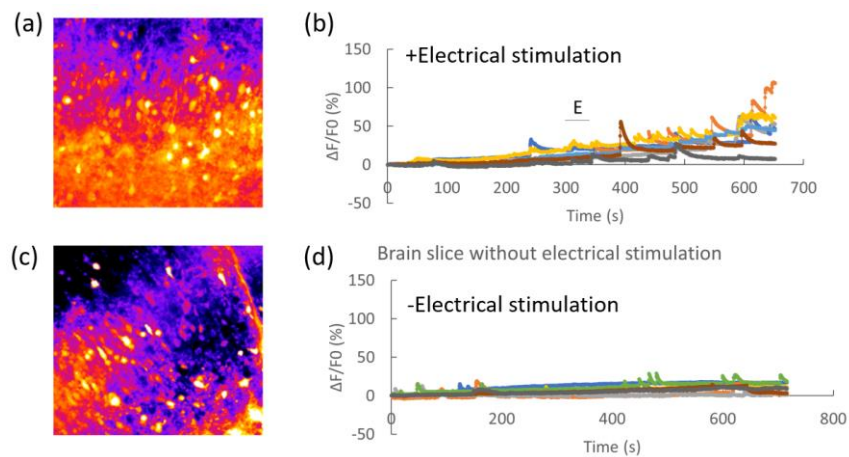
Figure 42 *Ex-vivo* study about brain response to electrical stimuli recorded by a calcium-sensitive dye. (a) Brain slice showed bright fluorescence after electrical stimulation. (b) Quantified fluorescence increasement of representative cells from (a). (c) Brain slice showed weak fluorescence before electrical stimulation. (d) Quantified fluorescence of representative cells from (c).

73
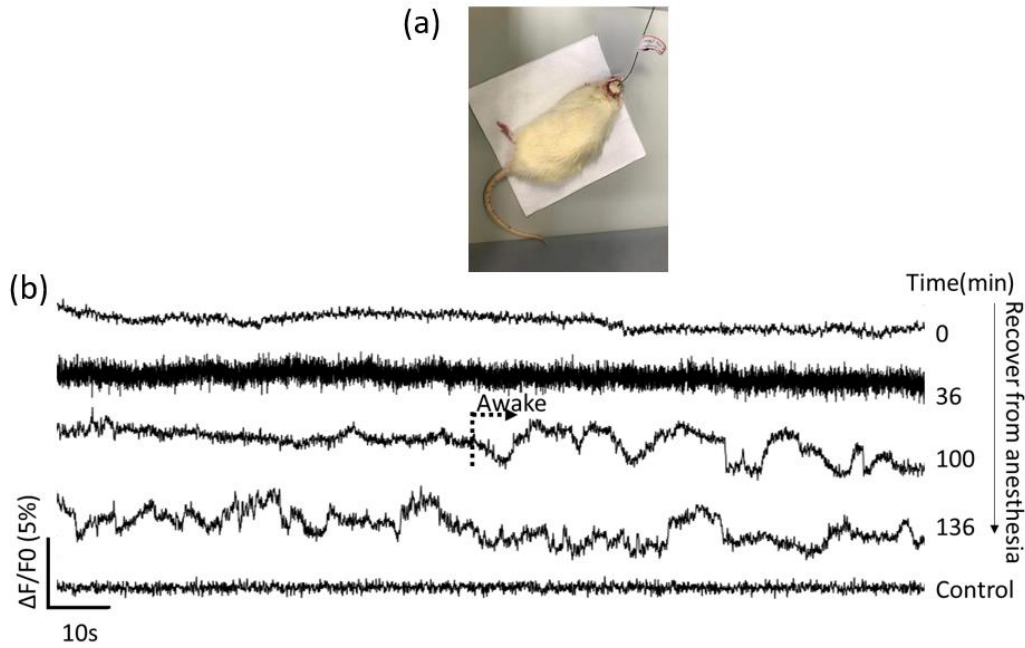
Figure 43 *In-vivo* recording of the calcium influx during head movements by the calcium-sensitive dye. Fiber photometry was used for recording fluorescence changes during the process that the rat recovered from its anesthetized state. After the awake time point, a fluorescence decrease matches a head turn left, and a fluorescence increase matches a head turn right.

By using this fluorescence calcium dye, we further conducted cellular experiments to compare the photoacoustic (PA) and fluorescence (FL) performance in monitoring the calcium response. As shown in Figure 44 a), the PA (red) signal and FL (green) signals generally mirror each other although with a little discordance induced by the difference in batches of cells or the inherent energy difference between PA and FL. Either without the dye (grey, PA ctr) or with the calcium inhibitor (dark green, FL), the signal amplitudes show little or no change upon stimulation. Compared to fiber photometry (Figure 44 d-e), one of the most widely used tools in neural science, the advantage that PA signal can be well detected through skull is obvious with ~1mm depth in the

experiment, while the fiber photometry can only collect signal when the fiber tip is extremely close to the cell surface.
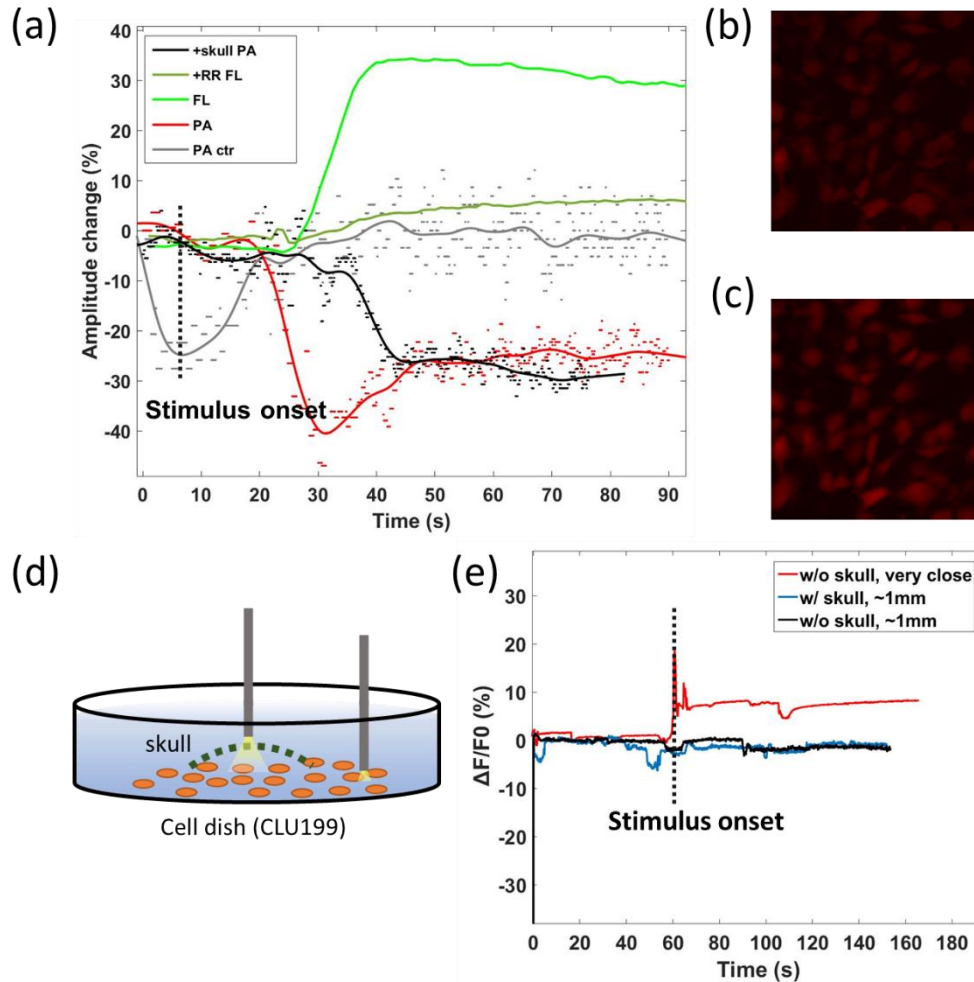
Figure 44 Photoacoustic signal is as reliable as fluorescence for detecting neural calcium response yet has additional advantage of going deep through skull. (a) Cellular experiments by using a commercial fluorescence microscope and a customized photoacoustic setup for comparing the capability of photoacoustic in capturing neural calcium dynamics. RR: Calcium inhibitor; (b) Fluorescence image of the CLU199 cell before and (c) after stimulation. (d) Experimental setup by using fiber photometry. A skull was included or not included in two individual experiments with ~1mm distance; the fiber tip was very close to the dish bottom (cell surface) in a third experiment. (e) FL signals got from fiber photometry.

An integrated system was built to simultaneously record fluorescence and photoacoustic signal for *in vitro* study. As shown in Figure 45, a delay generator with

precise time control was used for sequential triggering of the laser output, the camera recording, and the electrical pulse from a function generator for neural stimulation. 532nm pulsed laser was introduced to an inverted fluorescence microscope for generating both PA and FL signals, and at the same time to trigger the oscilloscope to start recording and delivering signal to a computer. PA signal was amplified first by an ~20dB amplifier and then delivered to the oscilloscope, while FL signals are directly recorded by an sCMOS camera and can be analyzed by propriety software on the computer.
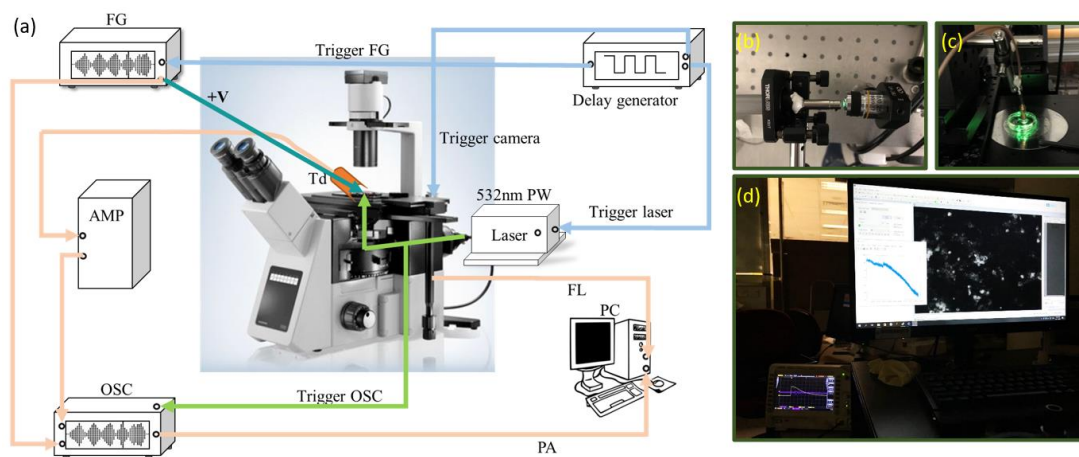
Figure 45 (a) An integrated system for simultaneous recording of photoacoustic and fluorescence signals for *in vitro* study. (b) The photo of pulsed laser alignment. (c) The photo showing PA excitation by the pulsed 532nm laser and recording by a transducer on cell culture. (c) Display interface showing simultaneous PA and FL recording.

For simultaneous *in vivo* recording of PA and FL, basic hardware components are the same as those shown in Figure 45 (a), whereas minor adjustments were made on the above system. As shown in Figure 46 (c) and (d), a fiber ferrule was inserted into a

hollow transducer for simultaneous collecting FL and PA signal, which was then fixed onto the mice head. The other end of the fiber was aligned to the objective of the microscope for delivering FL signal to the camera. The mouse was trained four days before the experiment to do locomotion to reduce acclimation noise during experiment (Figure 46 a)), and then injected with the calcium-sensitive dye which is validated previously in *ex-vivo* conditions (Figure 46 b)) following by inserting and fixing a fiber ferrule to the primary motor brain region. Simultaneous recording was then conducted during locomotion (Figure 46 e)) and the display interface show the real-time signal change (Figure 46 f)). Final data can all be stored and analyzed through MATLAB (Figure 46 g)).
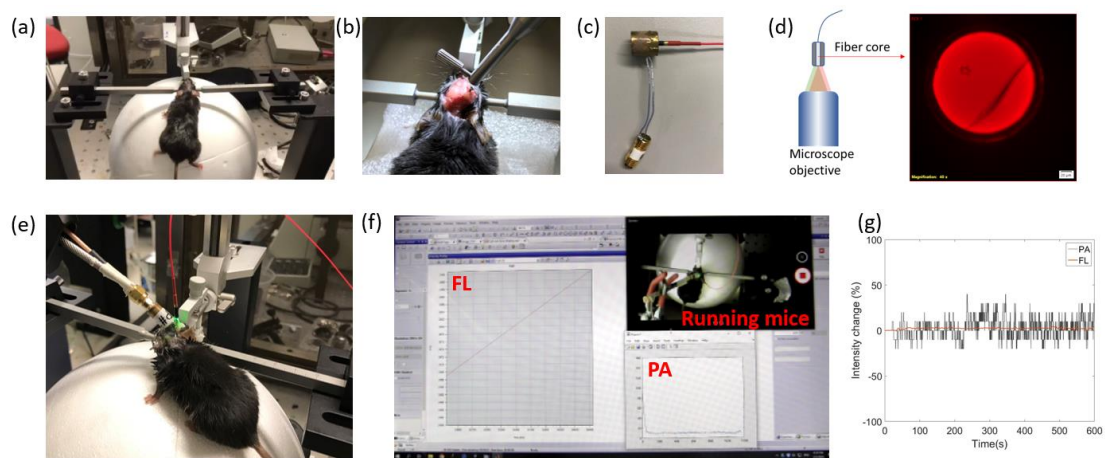
Figure 46 simultaneous recording of PA and FL during locomotion.

As blood has significant brighter PA signal than most of other absorbers in vivo, we here propose to use a fast multiwavelength source for spectrally scanning the absorbers and thus discriminate different signals in tissue. This source can potentially be provided

by work from reference[150]. As described in their updated work, the 532 nm pumped fiber laser source can provide five wavelengths, 532nm, 545nm, 558nm, 590nm, and 620nm with 1Mhz repetition rate and 150ns switching time, which is fast enough to capture a same event inside the physiological environment.

Prior to *in vivo* experiment, we first theoretically assessed the capability of the spectral unmixing method for solving this problem. Spectra of blood, dye and their mixture were scanned by a microplate reader and ratio of dye concentration in the mixture was calculated by matrix inverse calculation. Figure 47 shows the whole spectra of dye, blood, and dye mixed with blood. The extinction coefficients of both dye and blood (oxyhemoglobin) are calculated according to equation and compared in Table 4:

$$OD = \epsilon \times c \times l \quad (7)$$

Where ϵ is the extinction coefficient (L/(mol*cm)), c is the concentration (mol/L), and l is the length of the absorption pool(cm). It turns out that the dye and blood have no big difference in their ability to extinct light with both coefficient at 10^4. By changing the dye concentration and using a spectral unmixing algorithm, proportion of dye in the mixture can be calculated (Figure 48), with 4μM as the minimum concentration that can be discriminated in the mixture. This demonstrates that this method can be readily used in *in vivo* study where a dye concentration of 4μM is recommended in injection.
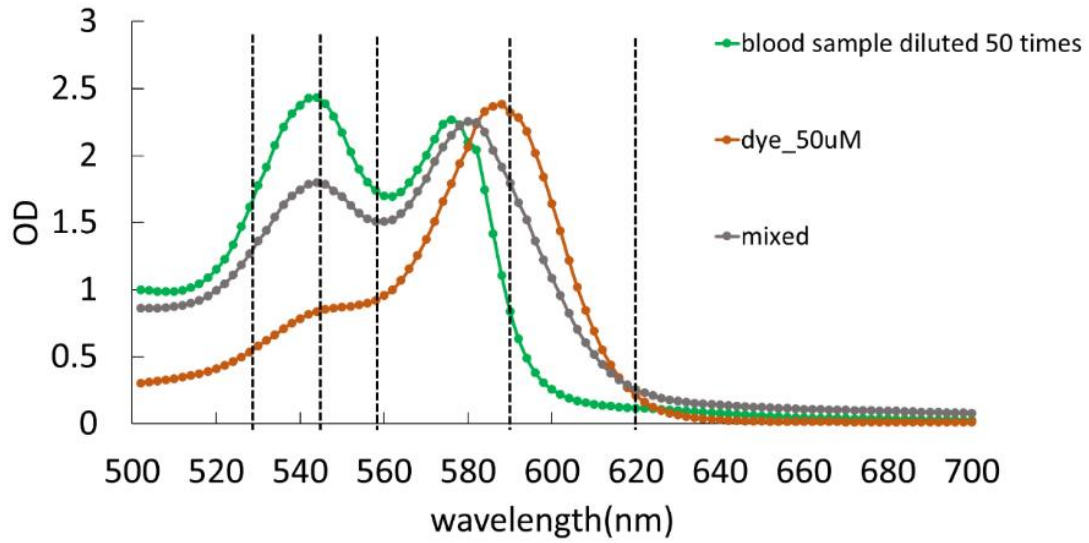
Figure 47 Spectra of dye, blood, and dye mixed with blood.

Table 4 Extinction coefficients of Oxyhemoglobin and Dye.

Wavelength (nm)	532	545	558	590	620
Oxyhemoglobin	4.8×10^4	5.1×10^4	3.3×10^4	5×10^4	3.2×10^4
Dye	2.7×10^4	3.4×10^4	4×10^4	9×10^4	5.7×10^4
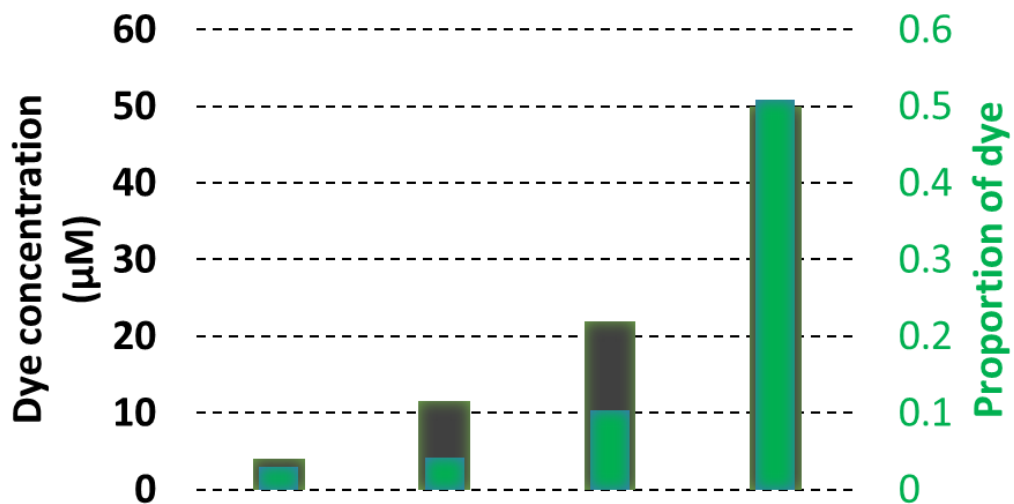
Figure 48 Proportion of dye (green) increases in the mixture with increasing dye concentration (black).

4. Summary and discussion

Photoacoustic imaging is an ideal way of circumventing scattering induced problems while retain advantages provided by optics. Photoacoustic imaging act as an ideal tool for combining vascular imaging and neural activity imaging in awake and behaving rodents, which lay a foundation for profound investigation for studying neurovascular relationship and obtaining reliable neuronal information in a noninvasive way at deep brain region. Preliminary data has suggested feasibility of this study. Improvements in the engineering side, including the wearable device configured with multiwavelength imaging and algorithm, imaging quality, imaging speed, application of GECI and appropriate behaving models, are remained to be done. Compared to a bench top PAM system, a system that aims to work during naturalistic behavior is deemed to need unique requirements from the perspectives of weight, animal acclimation, packaging and assemble of small optical components (especially those interact with the transducer), quality of signals collected by small and hollow transducer, wiring, etc.

It is important that the device should be light so that the animal does not feel heavy and uncomfortable. 8g seems light enough for rat, but for mice with smaller body structure and weight, novel probes remain to be designed. For example, a substitution of conventional bulky transducer can be the coverslip based transparent micro-ring acoustic detector (MRR)[151], a schematic illustration is shown in Figure 49. While MRR has only sub-millimeter size, it permits a larger detection angle of ultrasound

signal than piezoelectric transducers, which is favorable in providing larger field-of-view (FOV) in laser scanning PAM systems. Apart from small size, MMR features much broader ultrasonic detection bandwidth, which subsequently improves the axial resolution in PAI. The axial resolution, in our scheme, however, will be much worse due to the much-decreased bandwidth of the piezoelectric transducer with a hollow center. In addition, with using the MRR, the numerical aperture of the converging lens can be tighter as there will be no worry about whether the working distance is large enough for placing a transducer there, thus the lateral resolution can be improved. At last, as light oscillates orders of magnitude faster than ultrasonic waves, this light-based detection method thus allows highly sensitive detection over a wide frequency band. In this case, the SNR can be significantly improved.
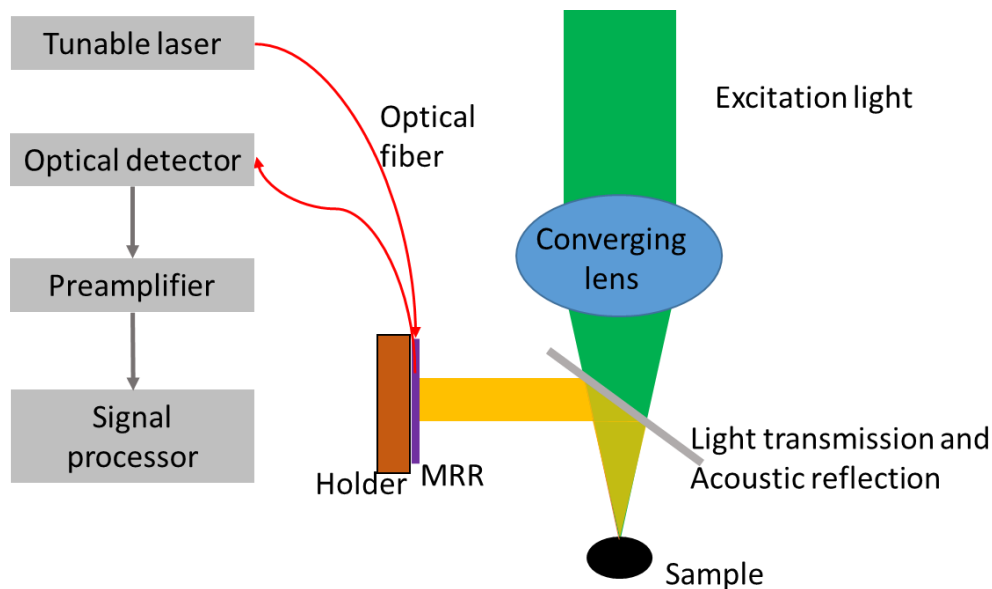
Figure 49 Schematic illustration of photoacoustic microscopy by using a micro-ring resonant filter.

In the current study, we use spectral unmixing method to extract dye concentration in the dye/blood mixture. Appropriate modification of the algorithm may favor more accurate and sensitive resolving. In addition of this, the signal-to-noise ratio (SNR) in calcium detection could also be improved with larger number of stimuli, instead of one stimulus each time. Another way considered for stripping the blood background is to separate by response time as in normal case, neural responses much faster than blood, which has also been exploited in other studies[152]. This method, however, put a lot of demands on the system imaging speed, which is a big challenge for small and wearable OR-PAM. Except for taking advantage of latency in temporal entanglement, it has also been demonstrated that there are brain regions that neurons response alone with no detectable blood response, which is termed neurovascular decoupling[153] and may also act as an investigation target.

In the current study, a calcium-sensitive dye with maximum excitation wavelength at 570nm was used. And the PA amplitude is found to change inversely with changing of the fluorescent amplitude with similar percentage. This on the one side suggests that the PA signal is as reliable as the fluorescent signal in the demonstration. On the other side, it initiates development of other photoacoustic-professional calcium-sensitive indicators, including dyes and proteins which emit PA signals those are proportional to the change of intracellular calcium concentrations. The decrease of PA amplitude and with increased intracellular calcium influx can be explained in different aspects. First,

it may be induced by the reduced absorption upon calcium binding[154]. Secondly, it may result from shifted absorption peak upon calcium binding[155]. Thirdly, neither of the above two changed, but the competition between the energy for generating fluorescent and photoacoustic signal lead the result. Any one of these three process could be potential entry point for development of new photoacoustic calcium indicators.

Finally, device stability and recording reproducibility are important issues. In the naturalistic state, the animal may feel uncomfortable with the wearable device, and thus induce acclimation noise during recording. To this end, a device holder is designed and semi-permanently fixed on the skull and the rest of the system is worn only before experiment. There may also exist spontaneous behavior induced noise besides a designed behaving model, which is inevitable but can be reduced with multiple trainings before experiment and rather be ignored with multiple experiments. In the behaving state, fluctuations in blood pressure or heart rate can be the third factors that affect the reproducibility. The influence may be remarkable if the subject feels nervous and stressed. In all, acclimation is highly needed before any behaving studies to get reliable results under designed conditions.

Chapter 4　Conclusion and outlook

This thesis aims to push development of the neural science toolbox a small step forward. A basic scientific question underlying is the strong light scattering in biological tissue, which greatly impedes applications of optical techniques in neuroscience in deep brain. In this thesis, a photonic nanojet based microsphere enhanced optogenetic neural stimulation method and a photoacoustic neural recording method are demonstrated aiming to circumvent the light scattering attenuation in brain tissue. In the first study, simulation results show that the converging ability of microsphere provide a highly localized electromagnetic field within which the light intensity can be enhanced about four times and to a large extent complements the scattering induced loss of power density in the targeted brain region. Then experiments are systematically conducted from *in vitro*, *ex vivo*, to *in vivo* scenarios. The results showing favorable for eliciting comparable neural response with lower incident light power and thus less side effects, and the potential also exists in by using the same power but reach a deeper brain region. In the second study, the scattering-tolerant photoacoustic effect is introduced and exploited, and a wearable photoacoustic device is designed and fabricated. Feasibility of the idea is demonstrated *in vitro* and *in vivo* for photoacoustic monitoring of neural activity by calcium imaging, and the remaining work for further developments are discussed.

The combination of stimulation and imaging has potential to provide an invaluable tool

for precise monitoring and controlling neural activity to decipher the function of neural circuits in a causal way. All optical ways such as by using two photon optogenetics and two photon calcium imaging has been an emerging concept with developing of light-sensitive actuators, red-shifted neural activity indicators, closed-loop system design and algorithms, and news optical configurations. By changing pure optical reading to photoacoustic reading, extra benefits brought by photoacoustic are easily obtained. A system design is shown in Figure 50 adapting from Figure 40.
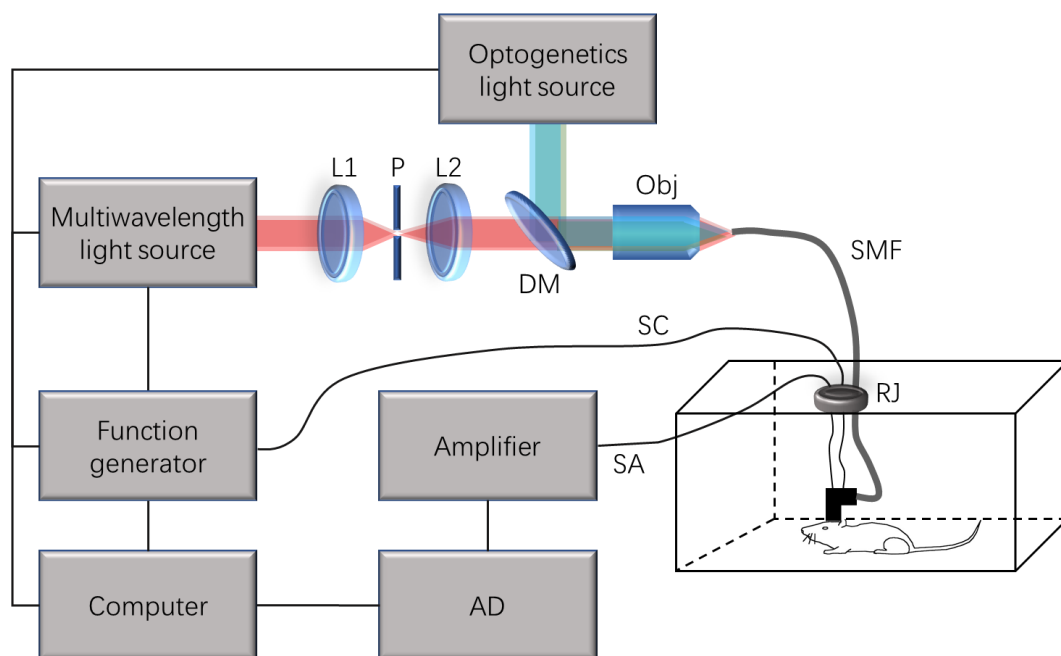
Figure 50 Design for closed-loop microsphere-enhanced optogenetics and photoacoustic imaging system. L1-L2, lens. P, pinhole. DM, dichroic mirror. Obj, objective. SMF, single-mode fiber. RJ, rotary joint. SC, scanning control. SA, signal acquisition. AD, analog to digital converter.

Conventionally single-mode fiber (SMF) which delivers TEM00 mode is required for high-resolution imaging. Due to limited efficiency of SMF, high incident power is needed for performing optogenetics. Microspheres therefore can work as a relay. The

multiwavelength light source in this system could potentially be a LED-array based light source, which is much more convenient and faster than lasers for tuning wavelengths. Given current technical context, imaging paths mainly used red-shifted wavelengths, and optogenetics are based on blue and green wavelengths. Recorded PA signal from the AD can be used as feedback for next round optogenetic experiment. Considering real-time requirements in a closed loop experiment, the MEMS mirror in the head-mounted device can be replaced by a digital micromirror device (DMD) which enables pattern generation and multi-spot stimulation. Due to the converging ability of microsphere, the beam path after reflected by DMD inside the device does not have to be refocused to a diffraction-limited spot like in a conventional OR-PAM does.

The combination of microsphere enhanced optogenetics with photoacoustic neural recording will undoubtfully facilitate functional study of the deep brain with opening the gate of combining of blood response with neural response in a high spatiotemporal scale. The first thing that comes to mind is this combination should facilitate profound dissection of the relationship between neural activity and cerebral blood flow, i.e., the neurovascular coupling. Besides the basic understanding that energy demanding of neural activities initiating localized oxygen consumption and subsequential increased blood flow, it is desired to discriminate by which kind of cell the vascular response is induced, i.e., inhibitory neurons, excitatory neurons, or glia cells. Combining of cell-type specific and micro-sphere-enhanced optogenetics with blood-signal-sensitive and

GECI-sensitive photoacoustic imaging will dramatically increase our knowledge of neurovascular coupling strategy in the deep brain in a less harmful way. This application, in practice, requires spectral discrimination among the imaging contrast and optogenetic ion channel to minimize the cross talks.

References

1.   Hodgkin, A.L. and A.F. Huxley, Action Potentials Recorded from Inside a Nerve Fibre. Nature, 1939. **144**: p. 710.
2.   Bean, B.P., The action potential in mammalian central neurons. Nat Rev Neurosci, 2007. **8**(6): p. 451-65.
3.   Buzsaki, G., C.A. Anastassiou, and C. Koch, The origin of extracellular fields and currents--EEG, ECoG, LFP and spikes. Nat Rev Neurosci, 2012. **13**(6): p. 407-20.
4.   Storm, J.F., Action potential repolarization and a fast after-hyperpolarization in rat hippocampal pyramidal cells. The Journal of physiology, 1987. **385**: p. 733-759.
5.   Kamimura, H.A.S., et al., Ultrasound neuromodulation: mechanisms and the potential of multimodal stimulation for neuronal function assessment. Front Phys, 2020. **8**.
6.   Hochbaum, D.R., et al., All-optical electrophysiology in mammalian neurons using engineered microbial rhodopsins. Nat Methods, 2014. **11**(8): p. 825-33.
7.   Fan, L.Z., et al., All-Optical Electrophysiology Reveals the Role of Lateral Inhibition in Sensory Processing in Cortical Layer 1. Cell, 2020. **180**(3): p. 521-535 e18.
8.   He, B., Neural Engineering. Third ed. 2020: Springer.
9.   Jensen, J.E., et al., The use of transcutaneous neural stimulation and isokinetic testing in arthroscopic knee surgery. The American Journal of Sports Medicine, 1985. **13**(1): p. 27-33.
10.   Miocinovic, S., et al., History, Applications, and Mechanisms of Deep Brain Stimulation. JAMA Neurology, 2013. **70**(2).
11.   Jiang, J., H. Cui, and K. Rahmouni, Optogenetics and pharmacogenetics: principles and applications. American journal of physiology. Regulatory, integrative and comparative physiology, 2017. **313**(6): p. R633-R645.
12.   Rastogi, S.K., et al., Remote nongenetic optical modulation of neuronal activity using fuzzy graphene. Proceedings of the National Academy of Sciences, 2020. **117**(24): p. 13339.
13.   Tian, B., Nongenetic neural control with light. Science, 2019. **365**(6452): p. 457.
14.   Aravanis, A.M., et al., An optical neural interface: in vivo control of rodent motor cortex with integrated fiberoptic and optogenetic technology. J Neural Eng, 2007. **4**(3): p. S143-56.
15.   Cohen, M.X., Where Does EEG Come From and What Does It Mean? Trends in Neurosciences, 2017. **40**(4): p. 208-218.
16.   Shokoueinejad, M., et al., Progress in the Field of Micro-Electrocorticography. Micromachines, 2019. **10**(1): p. 62.

17.   Obien, M.E., et al., Revealing neuronal function through microelectrode array recordings. Front Neurosci, 2014. **8**: p. 423.

18.   Zhao, Y., et al., Patch clamp technique: Review of the current state of the art and potential contributions from nanoengineering. Proceedings of the Institution of Mechanical Engineers, Part N: Journal of Nanoengineering and Nanosystems, 2009. **222**(1): p. 1-11.

19.   Croft, R.J. and R.J. Barry, Removal of ocular artifact from the EEG: a review. Neurophysiologie Clinique/Clinical Neurophysiology, 2000. **30**(1): p. 5-19.

20.   Bédard, C., H. Kröger, and A. Destexhe, Model of low-pass filtering of local field potentials in brain tissue. Physical Review E, 2006. **73**(5): p. 051911.

21.   Smith-Bindman, R., Is Computed Tomography Safe? New England Journal of Medicine, 2010. **363**(1): p. 1-4.

22.   Eggebrecht, A.T., et al., Mapping distributed brain function and networks with diffuse optical tomography. Nature photonics, 2014. **8**(6): p. 448-454.

23.   Tsai, L.L., et al., A Practical Guide to MR Imaging Safety: What Radiologists Need to Know. RadioGraphics, 2015. **35**(6): p. 1722-1737.

24.   Mace, E., et al., Functional ultrasound imaging of the brain: theory and basic principles. IEEE Transactions on Ultrasonics, Ferroelectrics, and Frequency Control, 2013. **60**(3): p. 492-506.

25.   Deffieux, T., et al., Functional ultrasound neuroimaging: a review of the preclinical and clinical state of the art. Current Opinion in Neurobiology, 2018. **50**: p. 128-135.

26.   Fork, R.L., Laser Stimulation of Nerve Cells in Aplysia. Science, 1971. **171**(3974): p. 907.

27.   Hirase, H., et al., Multiphoton stimulation of neurons. Journal of Neurobiology, 2002. **51**(3): p. 237-247.

28.   Yuste, E.M.C.R., Stimulating neurons with light. Current Opinion in Neurobiology, 2002(12): p. 587-592.

29.   Method of the Year 2010. Nature Methods, 2010. **8**(1): p. 1-1.

30.   Mohanty, S.K. and V. Lakshminarayananan, Optical Techniques in Optogenetics. J Mod Opt, 2015. **62**(12): p. 949-970.

31.   Lima, S.Q. and G. Miesenböck, Remote Control of Behavior through Genetically Targeted Photostimulation of Neurons. Cell, 2005. **121**(1): p. 141-152.

32.   Banghart, M., et al., Light-activated ion channels for remote control of neuronal firing. Nature Neuroscience, 2004. **7**(12): p. 1381-1386.

33.   Zemelman, B.V., et al., Photochemical gating of heterologous ion channels: Remote control over genetically designated populations of neurons. Proceedings of the National Academy of Sciences, 2003. **100**(3): p. 1352.

34.   Zemelman, B.V., et al., Selective Photostimulation of Genetically ChARGed Neurons. Neuron, 2002. **33**(1): p. 15-22.

35. Boyden, E.S., et al., Millisecond-timescale, genetically targeted optical control of neural activity. Nat Neurosci, 2005. **8**(9): p. 1263-8.

36. Zhang, F., et al., Multimodal fast optical interrogation of neural circuitry. Nature, 2007. **446**(7136): p. 633-639.

37. Gong, X., et al., An Ultra-Sensitive Step-Function Opsin for Minimally Invasive Optogenetic Stimulation in Mice and Macaques. Neuron, 2020. **107**(1): p. 38-51 e8.

38. Berndt, A., et al., Structure-Guided Transformation of Channelrhodopsin into a Light-Activated Chloride Channel. Science, 2014. **344**(6182): p. 420.

39. Berndt, A., et al., Bi-stable neural state switches. Nature Neuroscience, 2009. **12**(2): p. 229-234.

40. Gunaydin, L.A., et al., Ultrafast optogenetic control. Nat Neurosci, 2010. **13**(3): p. 387-92.

41. Mager, T., et al., High frequency neural spiking and auditory signaling by ultrafast red-shifted optogenetics. Nature Communications, 2018. **9**(1): p. 1750.

42. Lin, J.Y., et al., ReaChR: a red-shifted variant of channelrhodopsin enables deep transcranial optogenetic excitation. Nature neuroscience, 2013. **16**(10): p. 1499-1508.

43. Guru, A., et al., Making Sense of Optogenetics. Int J Neuropsychopharmacol, 2015. **18**(11): p. pyv079.

44. Pardridge, W., Targeted delivery of protein and gene medicines through the blood–brain barrier. Clinical Pharmacology & Therapeutics, 2015. **97**(4): p. 347-361.

45. Zhao, S., et al., Cell type–specific channelrhodopsin-2 transgenic mice for optogenetic dissection of neural circuitry function. Nature Methods, 2011. **8**(9): p. 745-752.

46. Wang, S., et al., Non-invasive, Focused Ultrasound-Facilitated Gene Delivery for Optogenetics. Scientific Reports, 2017. **7**(1): p. 39955.

47. Mihaela, A.S., et al., Safe and stable noninvasive focal gene delivery to the mammalian brain following focused ultrasound. Journal of Neurosurgery JNS, 2018. **130**(3): p. 989-998.

48. Kung, Y., et al., Focused shockwave induced blood-brain barrier opening and transfection. Scientific Reports, 2018. **8**(1): p. 2218.

49. Deverman, B.E., et al., Cre-dependent selection yields AAV variants for widespread gene transfer to the adult brain. Nature Biotechnology, 2016. **34**(2): p. 204-209.

50. Khakh, B.S. and M.V. Sofroniew, Diversity of astrocyte functions and phenotypes in neural circuits. Nature neuroscience, 2015. **18**(7): p. 942-952.

51. Saunders, A., et al., Molecular Diversity and Specializations among the Cells of the Adult Mouse Brain. Cell, 2018. **174**(4): p. 1015-1030.e16.

52. Zeisel, A., et al., Molecular Architecture of the Mouse Nervous System. Cell,

2018. **174**(4): p. 999-1014.e22.

53.   Ronzitti, E., et al., Recent advances in patterned photostimulation for optogenetics. Journal of Optics, 2017. **19**(11).

54.   Zorzos, A.N., E.S. Boyden, and C.G. Fonstad, Multiwaveguide implantable probe for light delivery to sets of distributed brain targets. Optics Letters, 2010. **35**(24): p. 4133-4135.

55.   Zorzos, A.N., et al., Three-dimensional multiwaveguide probe array for light delivery to distributed brain circuits. Opt Lett, 2012. **37**(23): p. 4841-3.

56.   Mahmoudi, P., H. Veladi, and F. Pakdel, Optogenetics, Tools and Applications in Neurobiology. Journal of Medical Signals & Sensors, 2017. **7**(2): p. 71-79.

57.   Adamantidis, A.R., et al., Neural substrates of awakening probed with optogenetic control of hypocretin neurons. Nature, 2007. **450**(7168): p. 420-424.

58.   Zhao, Y., et al., Wirelessly Operated, Implantable Optoelectronic Probes for Optogenetics in Freely Moving Animals. IEEE Transactions on Electron Devices, 2019. **66**(1): p. 785-792.

59.   Liu, C., et al., A wireless, implantable optoelectrochemical probe for optogenetic stimulation and dopamine detection. Microsystems & Nanoengineering, 2020. **6**(1): p. 64.

60.   Sparta, D.R., et al., Construction of implantable optical fibers for long-term optogenetic manipulation of neural circuits. Nat Protoc, 2011. **7**(1): p. 12-23.

61.   Yizhar, O., et al., Optogenetics in Neural Systems. Neuron, 2011. **71**(1): p. 9-34.

62.   Sutherland, B.A., T. Rabie, and A.M. Buchan, Laser Doppler flowmetry to measure changes in cerebral blood flow. Methods Mol Biol, 2014. **1135**: p. 237-48.

63.   Balardin, J.B., et al., Imaging Brain Function with Functional Near-Infrared Spectroscopy in Unconstrained Environments. Frontiers in human neuroscience, 2017. **11**: p. 258-258.

64.   Men, J., et al., Optical Coherence Tomography for Brain Imaging and Developmental Biology. IEEE journal of selected topics in quantum electronics : a publication of the IEEE Lasers and Electro-optics Society, 2016. **22**(4): p. 6803213.

65.   Kim, S.A., et al., Optical measurement of neural activity using surface plasmon resonance. Optics Letters, 2008. **33**(9): p. 914-916.

66.   Kao, F.-J., G. Keiser, and A. Gogoi, Advanced Optical Methods For Brain imaging. Vol. 5. 2019: Springer.

67.   Qin, Z., et al., Adaptive optics two-photon endomicroscopy enables deep-brain imaging at synaptic resolution over large volumes. Science Advances, 2020. **6**(40): p. eabc6521.

68.   Lai, P., et al., Photoacoustically guided wavefront shaping for enhanced optical focusing in scattering media. Nature photonics, 2015. **9**(2): p. 126-132.

69. Burette, A., et al., Knowing a synapse when you see one. Frontiers in neuroanatomy, 2015. **9**: p. 100-100.

70. Shen, F.Y., et al., Light microscopy based approach for mapping connectivity with molecular specificity. Nature Communications, 2020. **11**(1): p. 4632.

71. Kherlopian, A.R., et al., A review of imaging techniques for systems biology. BMC Syst Biol, 2008. **2**: p. 74.

72. Sparta, D.R., et al., Optogenetic strategies to investigate neural circuitry engaged by stress. Behavioural brain research, 2013. **255**: p. 19-25.

73. Vann, K.T. and Z.-G. Xiong, Optogenetics for neurodegenerative diseases. International journal of physiology, pathophysiology and pharmacology, 2016. **8**(1): p. 1-8.

74. Paz, J.T. and J.R. Huguenard, Optogenetics and epilepsy: past, present and future. Epilepsy currents, 2015. **15**(1): p. 34-38.

75. Etter, G., et al., Optogenetic gamma stimulation rescues memory impairments in an Alzheimer's disease mouse model. Nature Communications, 2019. **10**(1): p. 5322.

76. Moser, T. and A. Dieter, Towards optogenetic approaches for hearing restoration. Biochemical and Biophysical Research Communications, 2020. **527**(2): p. 337-342.

77. Simunovic, M.P., et al., Optogenetic approaches to vision restoration. Experimental Eye Research, 2019. **178**: p. 15-26.

78. Nussinovitch, U. and L. Gepstein, Optogenetics for in vivo cardiac pacing and resynchronization therapies. Nature Biotechnology, 2015. **33**(7): p. 750-754.

79. He, L., et al., Near-infrared photoactivatable control of Ca2+ signaling and optogenetic immunomodulation. eLife, 2015. **4**: p. e10024.

80. Grosenick, L., J.H. Marshel, and K. Deisseroth, Closed-loop and activity-guided optogenetic control. Neuron, 2015. **86**(1): p. 106-39.

81. Gradinaru, V., et al., Targeting and Readout Strategies for Fast Optical Neural Control In Vitro and In Vivo. The Journal of Neuroscience, 2007. **27**(52): p. 14231.

82. Park, S., et al., One-step optogenetics with multifunctional flexible polymer fibers. Nature Neuroscience, 2017. **20**(4): p. 612-619.

83. Canales, A., et al., Multifunctional fibers for simultaneous optical, electrical and chemical interrogation of neural circuits in vivo. Nature Biotechnology, 2015. **33**(3): p. 277-284.

84. Zhang, Z., et al., Closed-loop all-optical interrogation of neural circuits in vivo. Nat Methods, 2018. **15**(12): p. 1037-1040.

85. Kim, C.K., et al., Simultaneous fast measurement of circuit dynamics at multiple sites across the mammalian brain. Nat Methods, 2016. **13**(4): p. 325-8.

86. Forli, A., et al., Two-Photon Bidirectional Control and Imaging of Neuronal Excitability with High Spatial Resolution In Vivo. Cell Rep, 2018. **22**(11): p.

3087-3098.

87. Shemesh, O.A., et al., Temporally precise single-cell-resolution optogenetics. Nature Neuroscience, 2017. **20**(12): p. 1796-1806.

88. Tirlapur, U.K. and K. König, Targeted transfection by femtosecond laser. Nature, 2002. **418**(6895): p. 290-291.

89. Owen, S.F., M.H. Liu, and A.C. Kreitzer, Thermal constraints on in vivo optogenetic manipulations. Nat Neurosci, 2019. **22**(7): p. 1061-1065.

90. Bevilacqua, F., et al., In vivo local determination of tissue optical properties: applications to human brain. Appl Opt, 1999. **38**(22): p. 4939-50.

91. Yaroslavsky, A.N., et al., Optical properties of selected native and coagulated human brain tissues in vitro in the visible and near infrared spectral range. Physics in Medicine and Biology, 2002. **47**(12): p. 2059-2073.

92. Tuan Vo-Dinh, S.J.M., Optical methods and instrumentation in brain imaging and therapy. 2013: Springer.

93. Ait Ouares, K., et al., Opto nongenetics inhibition of neuronal firing. Eur J Neurosci, 2019. **49**(1): p. 6-26.

94. Stujenske, Joseph M., T. Spellman, and Joshua A. Gordon, Modeling the Spatiotemporal Dynamics of Light and Heat Propagation for In Vivo Optogenetics. Cell Reports, 2015. **12**(3): p. 525-534.

95. Long, M.A. and M.S. Fee, Using temperature to analyse temporal dynamics in the songbird motor pathway. Nature, 2008. **456**(7219): p. 189-194.

96. Kim, C.K., A. Adhikari, and K. Deisseroth, Integration of optogenetics with complementary methodologies in systems neuroscience. Nat Rev Neurosci, 2017. **18**(4): p. 222-235.

97. Chen, R., et al., Deep brain optogenetics without intracranial surgery. Nature Biotechnology, 2020.

98. Kennedy, S.H., M. Javanmard, and F.J. Vaccarino, A review of functional neuroimaging in mood disorders: positron emission tomography and depression. Can J Psychiatry, 1997. **42**(5): p. 467-75.

99. Slough, C., et al., Clinical Positron Emission Tomography (PET) Neuroimaging: Advantages and Limitations as a Diagnostic Tool. J Neuropsychiatry Clin Neurosci, 2016. **28**(2): p. A4, 67-71.

100. Mariani, G., et al., A review on the clinical uses of SPECT/CT. Eur J Nucl Med Mol Imaging, 2010. **37**(10): p. 1959-85.

101. Rosenthal, M.S., et al., Quantitative SPECT imaging: a review and recommendations by the Focus Committee of the Society of Nuclear Medicine Computer and Instrumentation Council. J Nucl Med, 1995. **36**(8): p. 1489-513.

102. Cabeza, R. and L. Nyberg, Imaging cognition II: An empirical review of 275 PET and fMRI studies. J Cogn Neurosci, 2000. **12**(1): p. 1-47.

103. van den Heuvel, M.P. and H.E. Hulshoff Pol, Exploring the brain network: a review on resting-state fMRI functional connectivity. Eur

Neuropsychopharmacol, 2010. **20**(8): p. 519-34.

104. Ma, Y., et al., Wide-field optical mapping of neural activity and brain haemodynamics: considerations and novel approaches. Philos Trans R Soc Lond B Biol Sci, 2016. **371**(1705).

105. Alexander, D. and M. Igor, Peer-to-peer Monte Carlo simulation of photon migration in topical applications of biomedical optics. Journal of Biomedical Optics, 2012. **17**(9): p. 1-3.

106. M.Born, E.W., Principles of Optics. 1997.

107. David A. Boas, D.H.B., Eric L. Miller, Charles A. DiMarzio, Misha Kilmer, Richard J. Gaudette, and Quan Zhang Imaging the body with diffuse optical tomography. IEEE Signal Processing Magazine, 2001.

108. London, I.C. Imaging and Metrology in biological tissue.

109. Yoon, S., et al., Deep optical imaging within complex scattering media. Nature Reviews Physics, 2020. **2**(3): p. 141-158.

110. Chen, R., et al., Deep brain optogenetics without intracranial surgery. Nat Biotechnol, 2020.

111. Pozzi, P., et al., Scattering Compensation for Deep Brain Microscopy: The Long Road to Get Proper Images. Frontiers in Physics, 2020. **8**(26).

112. Chen, Z., A. Taflove, and V. Backman, Photonic nanojet enhancement of backscattering of light by nanoparticles: a potential novel visible-light ultramicroscopy technique. Optics Express, 2004. **12**(7): p. 1214-1220.

113. Li, X., et al., Optical analysis of nanoparticles via enhanced backscattering facilitated by 3-D photonic nanojets. Optics Express, 2005. **13**(2): p. 526-533.

114. Heifetz, A., et al., Photonic Nanojets. J Comput Theor Nanosci, 2009. **6**(9): p. 1979-1992.

115. Kofler, J. and N. Arnold, Axially symmetric focusing as a cuspoid diffraction catastrophe: Scalar and vector cases and comparison with the theory of Mie. Physical Review B, 2006. **73**(23): p. 235401.

116. Chen, L., et al., Microsphere-Toward Future of Optical Microscopes. iScience, 2020. **23**(6): p. 101211.

117. Liu, X., et al., Selecting a Proper Microsphere to Combine Optical Trapping with Microsphere-Assisted Microscopy. Applied Sciences, 2020. **10**(9).

118. Zhang, X.A., I.T. Chen, and C.H. Chang, Recent progress in near-field nanolithography using light interactions with colloidal particles: from nanospheres to three-dimensional nanostructures. Nanotechnology, 2019. **30**(35): p. 352002.

119. Kong, S.-C., et al., Photonic nanojet-enabled optical data storage. OPTICS EXPRESS, 2008. **16**.

120. Zhu, J. and L.L. Goddard, All-dielectric concentration of electromagnetic fields at the nanoscale: the role of photonic nanojets. Nanoscale Advances, 2019. **1**(12): p. 4615-4643.

121. Chen, S., et al., Near-infrared deep brain stimulation via upconversion nanoparticle–mediated optogenetics. Science, 2018. **359**: p. 679-684.

122. Pietrobon, D., Calcium channels and channelopathies of the central nervous system. Mol Neurobiol, 2002. **25**(1): p. 31-50.

123. Berridge, M.J., P. Lipp, and M.D. Bootman, The versatility and universality of calcium signalling. Nature Reviews Molecular Cell Biology, 2000. **1**(1): p. 11-21.

124. Kovacs, K.J., c-Fos as a transcription factor] a stressful (re)view from a functional map. Neurochemistry International, 1998. **33**: p. 287-297.

125. Bolin, F.P., et al., Refractive index of some mammalian tissues using a fiber optic cladding method. Applied Optics, 1989. **28**: p. 2297-2303.

126. Pi, R., et al., Minocycline prevents glutamate-induced apoptosis of cerebellar granule neurons by differential regulation of p38 and Akt pathways. J Neurochem, 2004. **91**(5): p. 1219-30.

127. Kim, J.Y., et al., Intracerebroventricular viral injection of the neonatal mouse brain for persistent and widespread neuronal transduction. J Vis Exp, 2014(91): p. 51863.

128. Rivnay, J., et al., Next generation probes particles and proteins for neural interfacing. Science Advances, 2017. **3**.

129. Bangs Laboratories, I., Material Properties of Polystyrene and Poly(methyl methacrylate) (PMMA) Microspheres. Tech Support Doc 0021, Bangs Laboratories, Inc., 2015.

130. Bernard, C., Optogenetics: Keep Interpretations Light. eNeuro, 2020. **7**(2): p. ENEURO.0091-20.2020.

131. Kang, H., et al., Thermoplasmonic Optical Fiber for Localized Neural Stimulation. ACS Nano, 2020. **14**(9): p. 11406-11419.

132. Beard, P., Biomedical photoacoustic imaging. Interface focus, 2011. **1**(4): p. 602-631.

133. Attia, A.B.E., et al., A review of clinical photoacoustic imaging: Current and future trends. Photoacoustics, 2019. **16**: p. 100144.

134. Wang, L.V. and J. Yao, A practical guide to photoacoustic tomography in the life sciences. Nature Methods, 2016. **13**(8): p. 627-638.

135. Li, M., Y. Tang, and J. Yao, Photoacoustic tomography of blood oxygenation: A mini review. Photoacoustics, 2018. **10**: p. 65-73.

136. Jansen, K., G. van Soest, and A.F.W. van der Steen, Intravascular Photoacoustic Imaging: A New Tool for Vulnerable Plaque Identification. Ultrasound in Medicine & Biology, 2014. **40**(6): p. 1037-1048.

137. Longo, D.L., et al., Melanin-Based Contrast Agents for Biomedical Optoacoustic Imaging and Theranostic Applications. International Journal of Molecular Sciences, 2017. **18**(8).

138. Xu, Z., C. Li, and L.V. Wang, Photoacoustic tomography of water in phantoms

and tissue. Journal of biomedical optics, 2010. **15**(3): p. 036019-036019.

139. Wang, X., et al., Noninvasive laser-induced photoacoustic tomography for structural and functional in vivo imaging of the brain. Nature Biotechnology, 2003. **21**(7): p. 803-806.

140. Li, L., et al., Label-free photoacoustic tomography of whole mouse brain structures ex vivo. Neurophotonics, 2016. **3**(3): p. 035001-035001.

141. Olefir, I., et al., Spatial and Spectral Mapping and Decomposition of Neural Dynamics and Organization of the Mouse Brain with Multispectral Optoacoustic Tomography. Cell Reports, 2019. **26**(10): p. 2833-2846.e3.

142. Deán-Ben, X.L., et al., Functional optoacoustic neuro-tomography for scalable whole-brain monitoring of calcium indicators. Light: Science & Applications, 2016. **5**(12): p. e16201-e16201.

143. Yao, J. and L.V. Wang, Photoacoustic Brain Imaging: from Microscopic to Macroscopic Scales. Neurophotonics, 2014. **1**(1).

144. Tang, J., et al., Wearable 3-D Photoacoustic Tomography for Functional Brain Imaging in Behaving Rats. Scientific Reports, 2016. **6**(1).

145. Xi, L., et al., Hybrid photoacoustic and electrophysiological recording of neurovascular communications in freely-moving rats. NeuroImage, 2017. **161**: p. 232-240.

146. Chen, Q., H. Xie, and L. Xi, Wearable optical resolution photoacoustic microscopy. Journal of Biophotonics, 2019. **12**(8).

147. Deán-Ben, X.L., et al., Functional optoacoustic neuro-tomography for scalable whole-brain monitoring of calcium indicators. Light: Science &Amp; Applications, 2016. **5**: p. e16201.

148. Deán-Ben, X.L., et al., Functional optoacoustic neuro-tomography of calcium fluxes in adult zebrafish brain in vivo. Optics Letters, 2017. **42**(5): p. 959-962.

149. Shemetov, A.A., et al., A near-infrared genetically encoded calcium indicator for in vivo imaging. Nature Biotechnology, 2020.

150. Liu, C., Y. Liang, and L. Wang, Optical-resolution photoacoustic microscopy of oxygen saturation with nonlinear compensation. Biomedical Optics Express, 2019. **10**(6).

151. Li, H., et al., A transparent broadband ultrasonic detector based on an optical micro-ring resonator for photoacoustic microscopy. Sci Rep, 2014. **4**: p. 4496.

152. Gottschalk, S., et al., Rapid volumetric optoacoustic imaging of neural dynamics across the mouse brain. Nat Biomed Eng, 2019. **3**(5): p. 392-401.

153. Huo, B.X., J.B. Smith, and P.J. Drew, Neurovascular coupling and decoupling in the cortex during voluntary locomotion. J Neurosci, 2014. **34**(33): p. 10975-81.

154. Mishra, A., et al., Near-Infrared Photoacoustic Imaging Probe Responsive to Calcium. Anal Chem, 2016. **88**(22): p. 10790-10794.

155. Roberts, S., et al., Calcium Sensor for Photoacoustic Imaging. J Am Chem Soc,

2018. **140**(8): p. 2718-2721.